REPORT DOCUMENTATION PAGE

Form Approved
OMB No. 0704-0188

1. REPORT DATE *(DD-MM-YYYY)*	2. REPORT TYPE	3. DATES COVERED *(From - To)*
28-12-2006	Annual Research Summary	01-JUL-2005 - 30-SEP-2006

4. TITLE AND SUBTITLE
Coatings and Biodegradable and Bioasorbable Films

5a. CONTRACT NUMBER
N00014-04-1-0703

5b. GRANT NUMBER

5c. PROGRAM ELEMENT NUMBER

6. AUTHOR(S)
Shelby F. Thames and James W. Rawlins

5d. PROJECT NUMBER

5e. TASK NUMBER

5f. WORK UNIT NUMBER

7. PERFORMING ORGANIZATION NAME(S) AND ADDRESS(ES)
The University of Southern Mississippi
Southern Station Box 5157
Hattiesburg, MS 39406-5157

8. PERFORMING ORGANIZATION REPORT NUMBER

9. SPONSORING/MONITORING AGENCY NAME(S) AND ADDRESS(ES)
Office of Naval Research
875 N. Randolph St.
One Liberty Center
Arlington, VA 22203-1995

10. SPONSOR/MONITOR'S ACRONYM(S)

11. SPONSOR/MONITOR'S REPORT NUMBER(S)

12. DISTRIBUTION/AVAILABILITY STATEMENT

DISTRIBUTION STATEMENT A
Approved for Public Release
Distribution Unlimited

13. SUPPLEMENTARY NOTES

14. ABSTRACT

Research and development activities focused on environmentally friendly monomer, polymer and composite materials for Navy coating and packaging needs. Specifically focusing on the plasticizing effects of vegetable oil macromonomers as incorporated into emulsion polymers for efficient almost zero VOC film formation and the additional benefit of auto-oxidative polymerization after application. The resulting formulated coatings met or exceeded each of the specified Military specifications and are currently being evaluated for larger surface area application ease in combination with monomer and polymer scale up and commercialization. Polyesters and polyester-urethane block copolymers were evaluated for potential as biodegradable food packaging and pallet stretch wrap. The screening studies have resulted in materials with similar toughness as conventional materials and cursory data suggest acceptable biodegradability. Further evaluations will be performed in conjunction with the Natick Soldier Center. High throughput screening methods were evaluated as a precursor for ASTM 6691-01 testing and proved valuable by reducing the screening time from 20 days to 48 hours. Several areas of optimization, such as the types of bacterial organisms, were investigated where

15. SUBJECT TERMS

Environmentally friendly coatings, Topside Navy Haze Gray, Vegetable Oil Macromonomer, Low VOC, Biodegradable Food Packaging, Polyester-Polyurethanes, Pallet Stretch Wrap, block copolymer, Dendritic Aliphatic polyesters, Oxygen permeability, water vapor transmission

16. SECURITY CLASSIFICATION OF:			17. LIMITATION OF ABSTRACT	18. NUMBER OF PAGES	19a. NAME OF RESPONSIBLE PERSON
a. REPORT	b. ABSTRACT	c. THIS PAGE			James W. Rawlins
U	U	U		58	19b. TELEPHONE NUMBER *(Include area code)* 601-266-4781

ONR Annual Report from The University of Southern Mississippi

Abstract

Research and development activities focused on environmentally friendly monomer, polymer and composite materials for Navy coating and packaging needs. Specifically focusing on the plasticizing effects of vegetable oil macromonomers as incorporated into emulsion polymers for efficient almost zero VOC film formation and the additional benefit of auto-oxidative polymerization after application. The resulting formulated coatings met or exceeded each of the specified Military specifications and are currently being evaluated for larger surface area application ease in combination with monomer and polymer scale up and commercialization. Polyesters and polyester-urethane block copolymers were evaluated for potential as biodegradable food packaging and pallet stretch wrap. The screening studies have resulted in materials with similar toughness as conventional materials and cursory data suggest acceptable biodegradability. Further evaluations will be performed in conjunction with the Natick Soldier Center. High throughput screening methods were evaluated as a precursor for ASTM 6691-01 testing and proved valuable by reducing the screening time from 30 days to 48 hours. Several areas of optimization, such as the types of bacterial organism, were investigated where fluorescence was a most convenient method for microtiter plate detection. Excellent progress was made developing new nanocomposites and salt water triggered dissolution and degradation of polyester composites.

Project list

Environmentally Friendly Navy Haze Gray Coatings

Thames and Rawlins Pages 2-12

Polyesters and Polyester-Polyurethanes for Biodegradable Food Packaging and Pallet Stretch Wrap for the US Navy

Storey and Mauritz Pages 13-25

Novel Biodegradable Films Based on Cross-linked Dendritic Aliphatic Polyesters Containing Multiple Functional Hydroxyl Groups

Nazarenko Pages 26-34

Evaluation of Film Composition on Biodegradation

Wicks Pages 35-37

Highly Exfoliated Poly(ε-caprolactone)/Organo-montmorillonite Nanocomposites by in-Situ Polymerization

Mathias Pages 38-58

Environmentally Friendly Navy Haze Gray Coating
Shelby F. Thames and James W. Rawlins

Introduction

Naval ships require specialized coatings to combat severely corrosive marine environments. Naval coatings that come into contact with seawater possess anti-fouling properties to prevent fouling deposits from accumulating on the ship's surface. Specific to this project are other exterior coatings, termed Navy Haze Gray (NHG), that are applied to the ships topside forming an integral component of the ship's counter-measures weapons system. Apart from protecting topside mechanical equipment and structures from the weather, these coatings also provide visual camouflage by blending the ship into the open ocean background.

Current topside NHG coatings are formulated from solvent-based silicone-modified alkyds that contain high amounts of volatile organic compounds (VOCs). As an example, Interlac 2 supplied by International Marine Coatings has VOC levels of 336 g/L (2.80 lb/gal) at 60± 2% volume solids and a flash point of 100°F (Setaflash). Interlac 2 has a touch-dry time of 2 hours and hard-dry time of 8 hours at 77°F and meets MIL specification MIL-PRF-24635B (SH) LSA TYII CL2. Therefore, the objective of our research was to develop an environmentally-friendly waterborne coating with minimal odor and low-to-zero VOC content. Waterborne coatings deliver clean–up ease, reduced fire hazards, and low toxicity to DoD contractors or Navy personnel.

Historically our research group (Thames-Rawlins RG) has focused on research and development of environmentally responsible biobased technology such as vegetable oil derived monomers and cosolvent-free latexes produced via combinations of these monomers with conventional petroleum derivatives. The novel derivatives add value to our nation's agricultural industry while reducing our petroleum reliance. A novel class of vegetable oil macromonomers (VOMMs) were synthesized for utilization in cosolvent-free latexes. By design, VOMMs contain three separate and identifiable functionalities. First, the acrylic moiety through which free-radical initiated polymerizations can proceed; secondly, the C18 flexible hydrocarbon chain that functions as a powerful coalescing aid; and finally, the $-CH_2-$ flanked 9-10 olefinic double bond where oxidative polymerization is facilitated. In practice, the acrylate functionality allows for facile copolymerization of the VOMM with common monomers such as vinyl acetate, methyl methacrylate, methyl acrylate, butyl acrylate, styrene, and many more. After the VOMM is covalently bound to the polymer backbone, it is a non-fugitive plasticizing monomer and consequently the latex is odor-free and environmentally responsible requiring little to no organic solvents for efficient and durable film formation.

Monomer Synthesis

The source oil and type of VOMMs synthesized and evaluated in this project were varied in order to screen many variables efficiently. Linseed oil-based VOMMs were synthesized to take advantage of the oil's high unsaturation. The primary fatty acids contained in linseed oil are linolenic acid (50%), linoleic acid (18%), and oleic acid (21%) resulting in an iodine value of 165-185.

Urethane linseed acrylate monomer (ULiAM VOMM) was first evaluated in all-acrylic latexes. However, significant variation in monomer reproducibility and inconsistent latex results and thin film performance eliminated ULiAM for use in NHG coatings. A series of linseed oil and soy oil VOMMs were designed and synthesized including linseed acrylate monomer (LiAM), soy acrylate monomer (SAM), soy amide acrylate monomer (SoyAA-1), soy urethane acrylate monomer (SoyUA-1), linseed amide methacrylate monomer (LinMA-1), linseed amide acrylate monomer (LinAA-1), and soy amide methacrylate monomer (SoyMA-1). Figure 1 shows the representative structure of each of these monomers, and examples of the synthesis of ULiAM and LinAA-1 are given in the following paragraphs.

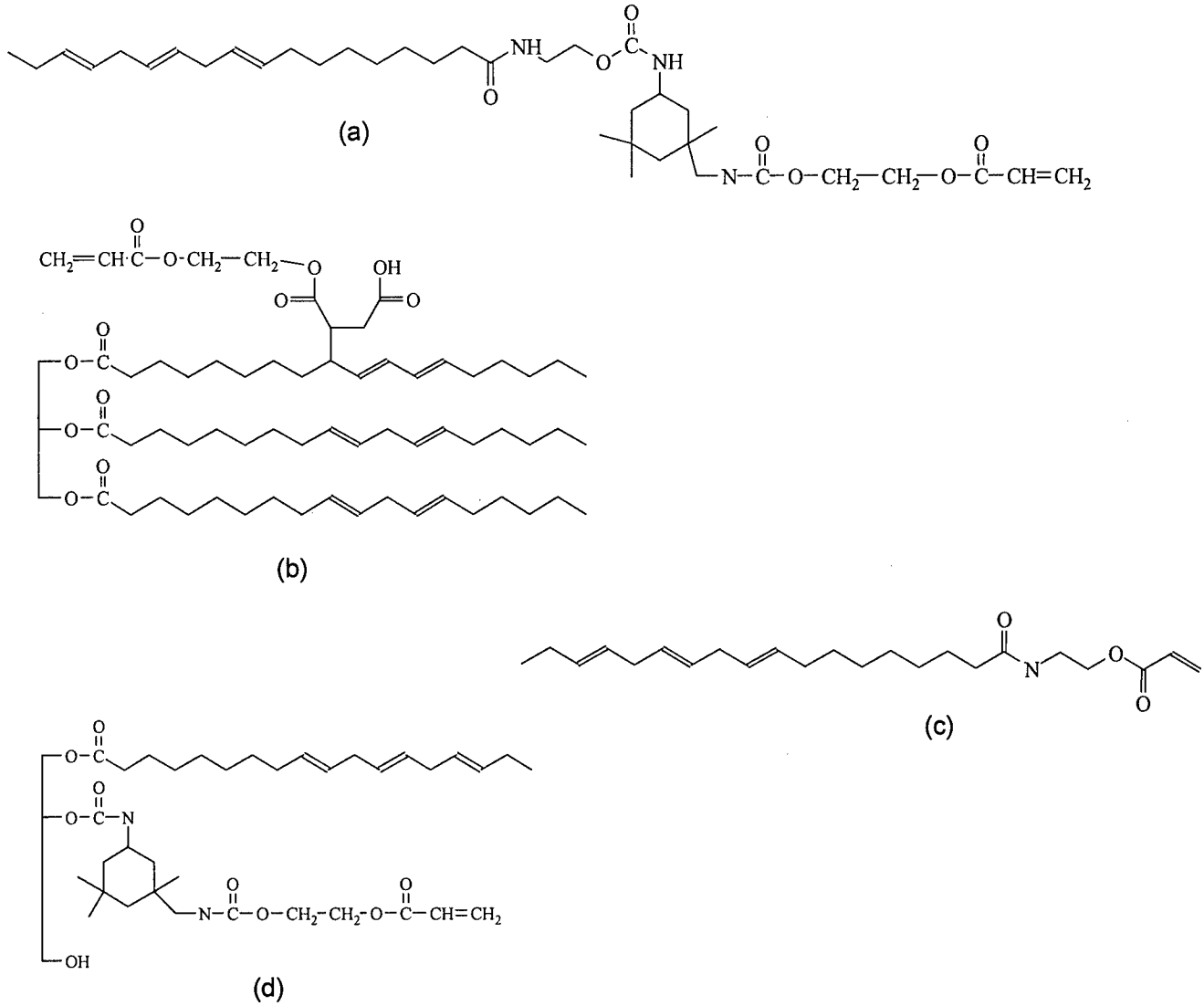

Figure 1. Representative structures of: (a) SoyUA-1/LinUA-1, (b) SAM/LiAM, (c) SoyAA-1/LinAA-1, and (d) ULiAM/USAM.

Synthesis of Urethane Linseed Acrylate Monomer (ULiAM)

A 1000 mL three-neck flask equipped with a thermocouple, condenser, mechanical stirrer, and nitrogen purge was charged with 1000.0 g of soybean oil, 0.5 g of Fascat® 4100, and 207.8 g of glycerol. Nitrogen was bubbled through the vegetable oil for 12 hours. The reaction was heated to 245°C and maintained for 4 hours under nitrogen atmosphere with constant stirring. The reaction was then cooled to ambient conditions and the glyceride product was washed, dried with magnesium sulfate, filtered, and characterized by gel permeation chromatography (GPC) and nuclear magnetic resonance (NMR).

A 500 mL three-neck flask equipped with a thermocouple, condenser, mechanical stirrer, and nitrogen purge was charged with 111.14 g isophorone diisocyanate (IPDI), 2.0 g dibutyltin dilaurate, and 0.18 g phenothiazine. 58.06 g of hydroxyethyl acrylate (HEA) was added dropwise over a period of 4 hours. The reaction was maintained at ambient temperature using a water bath. Once the HEA addition was complete, 200.0 g of glycerides from step 1 of the synthesis was added to the flask and the reaction was raised to 60°C. The reaction was monitored using Fourier transform infrared (FTIR) spectroscopy, and was deemed complete when the isocyanate peak (2160 cm^{-1}) disappeared. The product, ULiAM, was characterized using GPC and NMR.

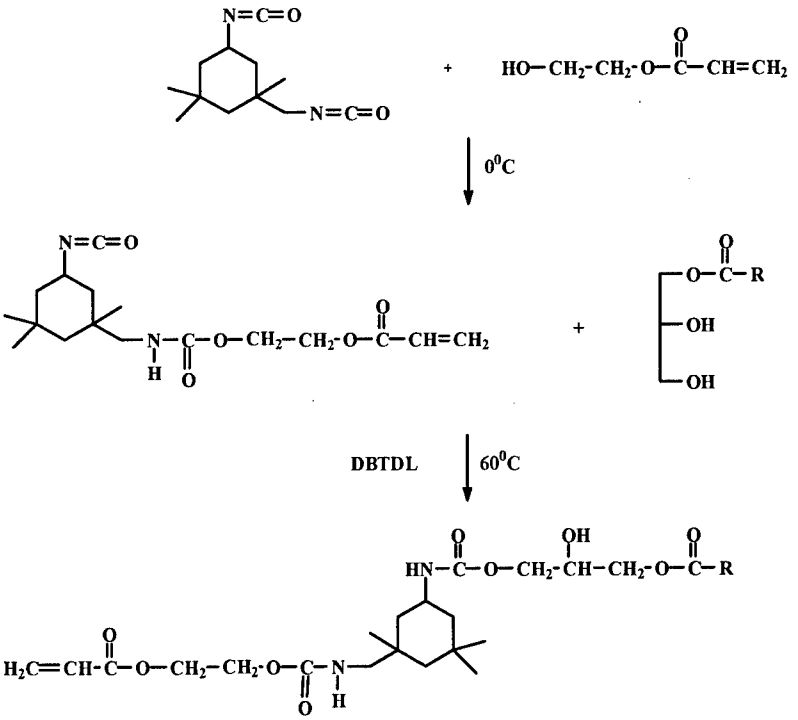

Figure 2. Linseed macromonomer synthesis.

Synthesis of Linseed Amide Acrylate Monomer (LinAA-1)

A 1000 mL three-neck flask equipped with a thermocouple, condenser, mechanical stirrer, and nitrogen purge was charged with 500.0 g linseed oil. Nitrogen was bubbled through the

vegetable oil for 12 hours. The oil was then heated to 60°C and sodium methoxide catalyst was added followed by *N*-methyl ethanolamine. The reaction was monitored via FTIR spectroscopy by following the disappearance of the ester peak and appearance of the amide peak. The product was then washed with brine solution to remove glycerol and excess *N*-methyl ethanolamine. After washing, the fatty amide product was dried with magnesium sulfate, filtered, and characterized by GPC and NMR.

A 500 mL three-neck flask equipped with mechanical stirrer, addition funnel, and temperature probe was charged with 250.0 g of the above fatty amide, 0.01 molar excess triethylamine (based on fatty amide equivalent weight), and 100.0 g methylene chloride. The flask was cooled to 0°C, and 70.0 g acryloyl chloride was added dropwise over 2 hours. The product was washed with brine solution to remove hydrochloric acid and other impurities, dried with magnesium sulfate, and the solvent removed by vacuum distillation. The product was characterized by GPC, high performance liquid chromatography (HPLC), gas chromatography-mass spectroscopy (GC-MS), and NMR.

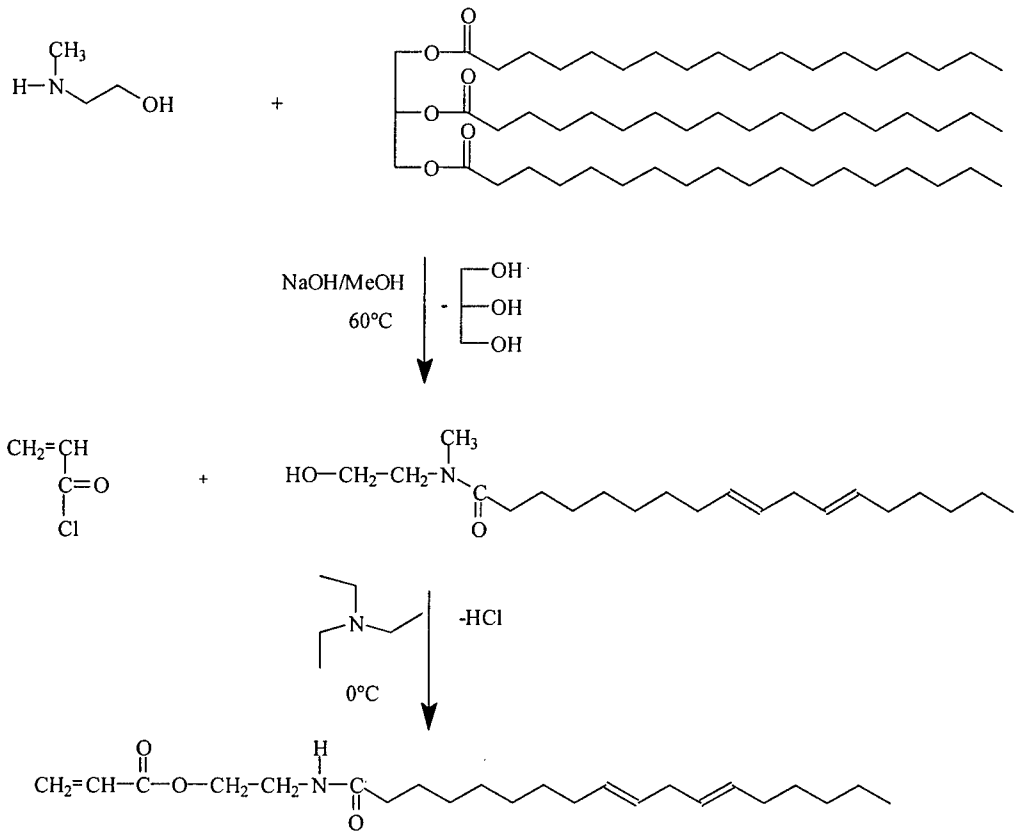

Figure 3. Linseed macromonomer synthesis.

Latex Synthesis

Latexes were synthesized in glass reaction kettles using a seeded, semi-continuous method in which both monomer and initiator were introduced into the reactor at a controlled rate using a Camile® 2000 automated data acquisition and control system. Manually programmed syringe

pumps were used to control initiator feed rate. The reaction temperature was controlled by partially submerging the reaction vessel in a water bath regulated at a constant temperature with an immersion circulator. A Claisen adapter was utilized to mount a nitrogen inlet and condenser. The remaining kettle lid openings were sealed with rubber septa. Initiator solutions and monomers were introduced into the reactor through needles placed in the septa, taking care to separate the needle tips. Table 1 shows an initial latex recipe.

Table 1. Emulsion Recipe

Water	454.50
Rhodapex® CD-128	13.40
Igepal® CO-887	3.70
Butyl acrylate	176.70
Methyl methacrylate	194.40
Methacrylic acid	5.46
Styrene	40.00
Diacetone acrylamide	9.20
Dytek® A	2.00
ULiAM	40.00
Sodium bicarbonate	1.85
Ammonium persulfate	7.30
Cumene hydroperoxide	0.15
Sodium metabisulfite	0.20
Adipic dihydrazide	4.60
Byk® 024	1.25
Kathon® LX 1.5	1.40
	956.11

Initial research suggested that a multistage polymerization process would provide latexes with the desired film properties. For this, the monomers were incorporated in two stages with the VOMM added in the second stage to provide good film coalescence. The monomers included in each stage were preemulsified with surfactant and water via mechanical agitation. The preemulsions were then added to the reaction using the recipe in Table 1.

It was noted that VOMMs had a considerable effect on overall monomer conversion during latex synthesis. The unsaturated fatty acids such as oleic acid, linoleic acid, and linolenic acid result in significant amounts of allylic protons. The allylic protons participate in chain transfer reactions resulting in a stabilized radical species and lower conversion. To overcome this effect, the emulsion polymerizations were conducted at 70°C for 16 hrs (~ 2.5 half-lives of the initiator, potassium persulfate at 70°C). In addition, a combination of water-soluble and oil-soluble free radical initiators (chasers) was added at the end of the polymerization to further reduce the residual monomer concentration. The resulting latexes had overall residual monomer values of < 1000 ppm, primarily butyl acrylate (slightly less than 500 ppm).

Recently, the latex synthesis process has been simplified to reduce the variation in the final latex, and better evaluate the VOMM influence on final coatings properties. The two-stage process was

simplified to a single-stage, semi-continuous, seeded emulsion polymerization. The seed was formed *in situ* as before and monomer was added directly to the kettle in the form of a preemulsion. Surfactant type, surfactant concentration, initiator type, and VOMM loading were evaluated at various levels. Table 2 presents the conditions and properties of the selected latexes and Table 3 shows a typical latex recipe.

Table 2. Conditions and Properties of Selected Latexes

Name	Surfactant Type	Surfactant Level	Control/VOMM	Initiator	Latex Properties	Drawdown Properties (Latex)	Drawdown Properties (Paint)
SLS 726-39	Sodium lauryl sulfate	2.27 phr	Control	APS	Viscous	Glossy, some cracks, foamy	Acceptable
SLS 726-49	Sodium lauryl sulfate	2.17 phr	Control	APS	Viscous, foamy	Cracks in film	Foam
SLS 726-51	Sodium lauryl sulfate	2.17 phr	Control	APS	Crashed	Not Formulated	Not Formulated
SLS 726-35	Sodium lauryl sulfate	2.17 phr	Control	APS	Acceptable	Glossy with some foam	Unusually foamy
SLS 726-50	Sodium lauryl sulfate	2.03 phr	Lin AA-1	APS	Viscous, foamy, some oil separation	Gritty (possibly foamy)	Foamy
SLS 726-36	Sodium lauryl sulfate	2.03 phr	Lin AA-1	APS	Some oil separation	Foamy, yellow tint	Very foamy, dull finish
SLS 726-37	Sodium lauryl sulfate	2.03 phr	Lin AA-1	APS	Some oil separation	Some foam	Some foam and spots
SLS 726-38	Sodium lauryl sulfate	1.97 phr	Lin AA-1	APS	Slightly viscous	Very foamy	Foamy, dull
SLS 726-47B	Sodium lauryl sulfate	1.65 phr	Lin AA-1	APS	Some oil separation	Cracks, yellow tint and foamy	Lots of black spots
SLS 726-33	Sodium lauryl sulfate	1.57 phr	control	APS	Acceptable	Foamy and glossy	Some foam
SLS 726-34	Sodium lauryl sulfate	1.44 phr	Lin AA-1	APS	Acceptable	Yellow, foamy, hazy	Some foam
SLS 726-40	Sodium lauryl sulfate	1.26 phr	Lin AA-1	APS	Slight oil separation	Cracks, yellow tint and foamy	Foamy
SLS 726-41	Sodium lauryl sulfate	0.67 phr	Lin AA-1	APS	Some oil separation	Very foamy, craters	Not Formulated
SLS 740-2	Sodium lauryl sulfate	2.50 phr	Lin AA-1	Redox	Some oil separation	Coalescing problems	Foamy with black spots
SLS 740-1	Sodium lauryl sulfate	2.03 phr	Lin AA-1	Redox	Acceptable	Hazy, poor appearance	Black spots
SLS 726-48	Sodium lauryl sulfate	1.65 phr	Lin AA-1	Redox	Acceptable	Very foamy	Some black spots
SLS 726-49	Rhodacal LDS-22	2.08 phr	Lin AA-1	Redox	Acceptable	Very glossy, acceptable	Acceptable
SLS 726-46	Rhodacal LDS-22	2.08 phr	Lin AA-1	APS	Dark oily appearance	Yellow, foamy, hazy	Some spots and foamy
SLS 726-50	Rhodacal LDS-22	2.36 phr	Lin AA-1	Redox	Some oil separation	Very foamy, glossy	Acceptable

Table 3. Optimized Emulsion Recipe

Water	540.00
Sodium lauryl sulfate	10.00
Butyl acrylate	206.00
Methyl methacrylate	204.60
Methacrylic acid	5.62
Styrene	40.00
Diacetone acrylamide	9.24
Dytek A	4.00
Linseed macromonomer	40.00
Sodium bicarbonate	1.85
Ammonium persulfate	1.80
t-Butyl hydroperoxide	0.30
Sodium metabisulfite	0.36
Adipic dihydrazide	9.20
	1072.97

Navy Haze Gray Coating

The NHG coating requires a specific blend of pigments to achieve the proper gray shade visually and according to NRL specifications. In Generations One and Two, this was accomplished by separately dispersing the individual blue, red, yellow, and white pigment in an aqueous medium with the appropriate additives. When the pigments are dispersed separately, color development with the individual shades is optimized, but the final coating often tends to exhibit flocculation. Generation Three (Table 4) was therefore designed with the colored pigments dispersed simultaneously.

Table 4. Mill Base Formulations

Colored Tint Base	
Water	117.05
Disperbyk® 191	24.95
BYK 021	3.22
Kathon LX 1.5%	0.32
AMP-95	0.32
Aerosil® 200	0.73
Red iron oxide	68.00
Yellow iron oxide	79.20
Phthalocyanine blue	25.53
White Tint Base	
Water	470.40
BYK 156	42.93

Natrosol® Plus 330	2.88
Ammonium hydroxide	5.60
Triton® CF-10	3.52
BYK 022	2.08
TiPure® 706	536.64
Huber 70C	536.64

The tint bases were properly dispersed to the required Hegman gauge, and formulated into the NHG coating (Table 5).

Table 5. Navy Haze Gray Coating

Colored tint base	4.67
White tint base	81.30
Water	48.78
Surfynol® 104A	0.49
Borchi™gel LW 44	4.67
Linseed VOMM latex	333.33
Optifilm® Enhancer 400	6.18
Tinuvin® 5151	3.46
BYK 325	0.17
Tributyl citrate	6.87

The coating viscosity was adjusted to 83-87 Krebs Units at 25°C. The UV absorber (Tinuvin 5151) was dissolved in the cosolvent (Optifilm Enhancer 400) for efficient blending and even incorporation.

The Generation Three coating was tested in our labs as per MIL-PRF-24635C and MIL-PRF-24596A, and the results are listed in Tables 6 and 7.

Table 6. Testing Results per MIL-PRF-24596A

Test No.	Description	Generation Three	Requirement
4.6.1	Pigment, weight %	10.59%	As specified by manufacturer
	Non-volatile vehicle solids wt %	48.20%	
	Volatile weight %	46.94	
	Mass per unit volume	1.125	
	Viscosity	78 KU	<100 KU
	Specular gloss @ 60°	52.5	45-60
	Hiding power (contrast ratio)	99.2	>90
4.6.1.2	Adhesion	Pass	Pass
4.6.2	Pot life	Not applicable	Not applicable
4.6.3	Drying time (minutes) @ 72° F		
	Set-to-touch	9	<120

	Dust free	10	<120
	Dry through	13	<480
	Dry hard	14	<480
4.6.3.1	Full hardness	7 days	
4.6.4	Volatile organic compound (VOC)	<15 g/L	<275 g/L
4.6.4.1	Class 3 submarine atmosphere volatiles	Classified	Classified
4.6.5	HAP content of coatings	None	<0.5-1.0
4.6.6	Hazardous pigments and additives	None	< 5 mg/L
4.6.6.1	Tantalum and tungsten content	None	<0.100
4.6.7	Yellowness (1 year)	Sample lost*	<3.0
4.6.8	Mixing properties	Pass	Pass
4.6.9	Spraying properties	Pass	Pass
4.6.10	Brushing properties	Pass	Pass
4.6.11	Flexibility	Pass	Pass
4.6.12	Knife test	Pass	Pass
4.6.13	Water resistance	Not applicable	Not applicable
4.6.14	Hydrocarbon fluid resistance	Not applicable	Not applicable
4.6.15	Salt spray resistance	Pass	Pass
4.6.16	Condensation blister resistance	Pass	# 8 Few
4.6.17	Exudate formation	Pass	Pass
4.6.18	Washability		
	60° gloss change	1.7	<50.0
4.6.19	Flash rust resistance	Pass	Pass
4.6.20	Recoatability	Sample lost*	Pass
4.6.21.2	Radiant panel test	Samples not evaluated.	
4.6.21.3	Smoke density chamber test		
4.6.21.4	Resistance to ignition		
4.6.21.5	Flashover determination		
4.6.21.6	Heat transfer		

* Test samples destroyed during hurricane Katrina.

Table 7. Coatings Test Results per MIL-PRF-24635B

Test No.	Description	Generation Three	Requirement
4.6.1	Condition in container	Pass	Pass
4.6.2.1	Partially full container	In progress**	Pass
4.6.2.2	Full container	In progress**	Pass
4.6.2.3	Accelerated storage stability	In progress**	Pass
4.6.3	Dilution stability	Pass	Pass
4.6.4	Brushing properties	Pass	Pass
4.6.5	Rolling properties	Pass	Pass
4.6.6	Spraying properties	Pass	Pass
4.6.7	Color		
	L*	55.88	56.0 ± 0.3

	a*	-1.72	-1.56 ± 0.3
	b*	-0.83	-1.37 ± 0.3
4.6.8	Odor	Slight odor	Not obnoxious or objectionable
4.6.9	Anchorage	Pass	Pass
4.6.10	Flexibility	Pass	Pass
4.6.11	Flake and crack resistance	Pass	Pass
4.6.12	Enamel recoatability	Sample lost*	Pass
4.6.13	Water resistance	#8 Few blisters	No blistering
4.6.14	Vehicle extraction	Not applicable	Not applicable
4.6.15	Silicone-alkyd copolymer resin	Not applicable	Not applicable
4.6.16	Specular gloss @ 60°	52.5	45-60
4.6.17	Drying time (minutes) @ 72° F		
	Set-to-touch	9	< 120
	Dust free	10	< 120
	Dry through	13	< 480
	Dry hard	14	< 480
4.6.18	Accelerated weathering (300 hours QUV)		
	Δ L*	0.36	≤ 1.0
	Δ a*	0.11	≤ 1.0
	Δ b*	-0.25	≤ 1.0
	Δ E*	0.45	≤ 1.0
	Gloss change @ 60°	7.20%	≤ 35%
4.6.19	Volatile organic compound (VOC)	< 15 g/L	< 275 g/L
4.6.20	Soluble and total metal content	Not applicable	Not applicable
4.6.20.1	Tantalum and tungsten content	Not applicable	Not applicable
4.6.21	Long term exterior exposure	Sample lost *	Pass
4.6.22	Flash point	Not applicable	Not applicable
	Water content	Not applicable	Not applicable
	Coarse particles	In progress	< 0.5
	Consistency	78 KU	< 100 KU
	Fineness of grind	7.0+	6+
	Contrast ratio	99.2	>90
4.6.23	Hazardous solvent content	None added	0.05-0.1 maximum

*Sample destroyed during hurricane Katrina.
**Testing due to finish August 2006.

NHG coatings Generations Two and Three were shared with Mr. Art Webb (Head, Marine Coatings Section Code 6138, Naval Research Laboratory, Washington DC) for evaluation as per MIL specifications, and his comments are reproduced below:

- Generation Two
  - Blocks even after 3 days of drying due to residual tack
  - Has poor spray properties, but good brush and drawdown properties
  - Is softer than Generation Three

- Coating viscosity is acceptable
- Condition in can is acceptable
- Odor is acceptable
- Ease of mixing is acceptable

- Generation Three
  - Does not block
  - Has good spray properties, but has poor brush and drawdown properties
  - Coating viscosity is acceptable
  - Condition in can is acceptable
  - Odor is acceptable
  - Ease of mixing is acceptable

Future Work

Currently, the linseed VOMM and the soy VOMM latexes are being reformulated to address the limitations expressed by Mr. Webb. During the second half of the project, film formation defects, termed black spots were observed in the final coating. We are investigating every step of our research from monomer synthesis to coating manufacture to identify the cause of the discoloration/pigment agglomeration. Once the defects are identified and eliminated, the latex will be scaled-up to 5-gallon batches and formulated into NHG Generation Four coating. We expect to send a gallon sample of Generation Four NHG coating for Mr. Art Webb's evaluation in the fourth quarter of 2006. Depending upon the results of the evaluation, the specific monomer and polymer designs will be scaled up to pilot plant sizes for monomer synthesis, emulsion polymer synthesis and coatings formulations for appropriate shipboard evaluation and testing.

Polyesters and Polyester-Polyurethanes for Biodegradable Food Packaging and Pallet Stretch Wrap for the US Navy

Personnel

This activity was conducted by Professors R.F. Storey (synthesis) and K. A. Mauritz (materials characterization). Synthesis personnel included T. Cooper and S. Moravek, both of whom are graduate students advised by Storey, and materials characterization personnel included Dr. M. Hassan, a post-doctoral associate working for Mauritz. Investigations of tailored material structure and properties were conducted in a materials optimization feedback loop with the synthesis component. Realistic tests of sample biodegradation were conducted in the Gulf of Mexico in collaboration with the USM Gulf Coast Research Laboratories (GCRL) (collaborators: D. Burke, J. Lotz, W. Hawkins). Trips were made to GCRL to facilitate and plan new tests and understand the nature of the seawater environment.

Synthesis and Characterization of Biodegradable Polyester Polyols and Model Compounds

Poly(D,L-lactide) (PDLLA) and poly(D,L-lactide-*co*-glycolide) (PLGA) were synthesized for use both as model compounds for structure/properties investigations and as polyols for TPU formulations. They were synthesized via Tin(II) 2-ethylhexyl octanoate (SnOct)-catalyzed bulk polymerization, using either 1,4-butanediol (BD), 1,2-propanediol (PD), or 2,2-bis(hydroxymethyl)butyric acid (BHMBA) as polymerization initiator. The use of BHMBA places a pendant carboxylic acid group along the backbone of the polyol, leading to an increased rate of water uptake and increased overall rate of degradation of the polyol.

Synthesis of PLGA polyol. The following is a representative procedure for the synthesis of a 50:50 (mol/mol), 2,000 g/mol PLGA polyol (Scheme 1), carried out under an inert N_2 atmosphere. D,L-lactide, 52.896 g, and glycolide, 42.598 g, were charged to a 2-necked 250 mL round bottom flask fitted with a mechanical stirrer comprising a 10 mm glass stir rod, a PTFE paddle, and a PTFE stir bearing. The reactor was submerged in a 150°C silicone oil bath, and the contents were stirred for 20 min to fully melt the monomers. Then, 4.506 g of BD and 0.034 g of SnOct were added to the flask, and the mixture was allowed to react with stirring for 3 h. The product was then poured into a storage container and stored under vacuum.

Synthesis of PDLLA polyol. The following is a representative procedure for the synthesis of a 2,000 g/mol PDLLA polyol. D,L-Lactide, 95.494 g, BD, 4.506 g, and SnOct, 0.034 g, were charged to a 1-necked 250 mL round bottom flask, which was then fitted with a mechanical stirrer comprising a 10 mm glass stir rod, a PTFE paddle, and a PTFE stir bearing. The reactor was submerged in a 130°C silicone oil bath, and the mixture was stirred for 5 h. The product was then poured into a storage container and stored under vacuum.

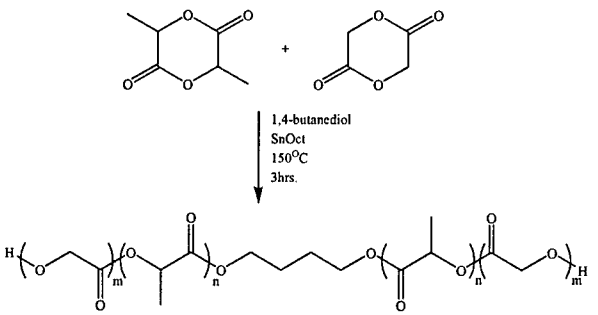

Scheme 1. Synthesis of poly(D,L-lactide-*co*-glycolide) (PLGA).

Synthesis of PDLLA diacid. PDLLA diols were converted to PDLLA diacids through reaction with excess succinic anhydride in the presence of a catalytic amount of N-methylimidazole at 70°C for 5 h in dichloroethane solution.

Synthesis of BHMBA-initiated PDLLA polyol. The following is a representative procedure for the synthesis of a 40,000 g/mol PDLLA polyol initiated from BHMBA. D,L-lactide (129 g, 0.893 mol) BHMBA (0.47 g, 3.17 mmol) and SnOct (0.14 g, 0.345 mmol) were added to a 250 mL, 1-neck round bottom flask equipped with an overhead stirrer. The polymerization was carried out by immersion of the flask in a 135° C thermostat-ed oil bath contained within the dry N_2 glove box, for 8 hr, after which the molten reactor contents were poured into a Teflon dish to cool. GPC characterization indicated that the actual number average molecular weight of the sample was 40,050 g/mol with a polydispersity of 1.24.

Synthesis of chain-extended BHMBA-initiated PDLLA. A BHMBA-initiated poly(D,L-lactide) was chain extended with L-lysine diisocyanate to create a model polyester with carboxylic acid pendent groups spaced regularly along the chain. The NCO/OH ratio was set to 1.02. To a 1-neck round bottom flask equipped with an overhead stirrer were charged 16.05 g (2.30 mmols) of BHMBA-PDLLA (target M_n=6595, experimental M_n=6985), 0.498 g (2.35 mmol) of LDI, 0.136 g (0.215 mmol) of dibutyltin dilaurate (DBTDL), and 60 mL of toluene. The polymerization was carried out by the immersion of the flask in a 40.0° C thermostated oil bath contained within a dry N_2 glove box, for 25 hr, after which the contents were allowed to cool. The polymer solution was then concentrated by removal of toluene under reduced pressure using a rotary evaporator and transferred into a Teflon dish. The dish and its contents were then put into a vacuum oven, to remove the remaining toluene, for 72 h or until a constant weight was obtained.

A molecular weight of 51,150 g/mol was achieved for the chain-extended BHMBA-PDLLA, which indicates a functionality of 7.3 acid pendent groups per molecule. Figure 1 depicts the shift to high molecular weight and the increase in polydispersity that occurred when the BHMBA-PDLLA was chain extended. The increase in polydispersity is a natural consequence of the step growth polymerization.

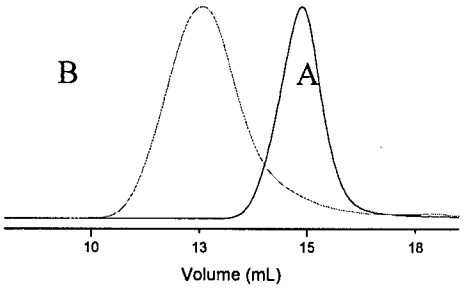

Figure 1. GPC chromatogram of BHMBA-PDLLA (A) and chain extended BHMBA-PDLLA (B).

Dielectric spectroscopic studies of degradation. Dielectric spectroscopy (DS) was used to interrogate chain biodegradation. For example, loss permittivity = ε" vs. frequency (f) spectra of an untreated (i.e., undegraded) 20,000 g/mol PDLLA diol sample were obtained at various temperatures and fitted to the Havriliak-Negami (HN) equation with the dc conductivity contribution in the region of low f subtracted (Figure 2). A well-defined maximum was observed and the peak maximum, f_{max}, increased with increasing temperature (T). This is a T_g - related relaxation associated with long range chain segmental mobility that starts around 50° C.

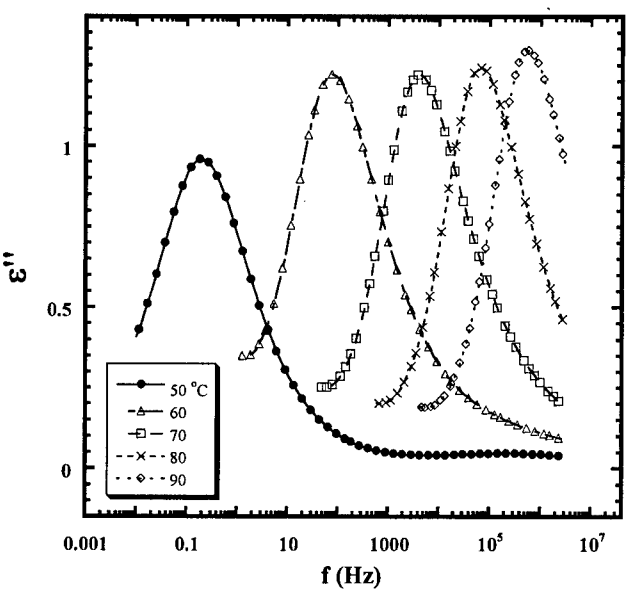

Figure 2. ε`` vs. log f, at various fixed temperatures for a dry undegraded sample with the dc conductivity contribution subtracted. The curves show an excellent fit of the HN equation to the data points.

A comparison between the α-relaxations at fixed temperature of 60° C for an untreated sample and corresponding sample that was degraded at 7.4pH at 37° C for 95 days is shown in Figure 3. At fixed T, the relaxation time $\tau_{max} = 1/(2\pi f_{max})$ decreases by decades reflecting more rapid chain motions (1). Note also that the peak is less symmetric for the non-degraded sample. The simple Rouse-Zimm model predicts that the relaxation time for long range chain motions in the rubbery state decreases with decreasing molecular weight. Hence, if the average molecular weight shifts to lower values through degradation, f_{max} will necessarily shift to higher values. This is the essential link between degradation by chain scission and dielectric relaxation spectra.

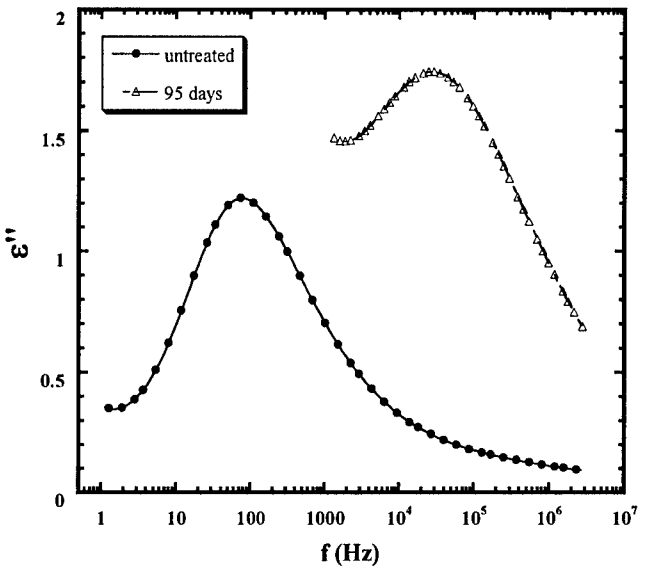

Figure 3. ε`` vs. log f at 60° C for dry untreated and 95d degraded samples with the dc conductivity contribution subtracted.

Values of τ_{max} at different temperatures extracted by fitting the HN equation to the DS data were used to construct Vogel-Fulcher-Tammann-Hesse (VFTH) plots for the degraded and undegraded samples; these plots are shown in Figure 4.

The plots are nonlinear, i.e., non-Arrhenius like. Also, there is a distinct separation between the curves for the non-degraded and degraded samples. The VFTH equation can be well fitted to the data for both degraded and non-degraded samples as in cases for temperatures above the α-transition for other polymers. Curve-fitted values of the Vogel temperature (T_V) decreased with immersion in buffer solution for 95 d. T_V, which is often related to the glass transition but occurs at lower temperatures, would be expected to decrease with increased degradation time as the free volume increases, as is the case here.

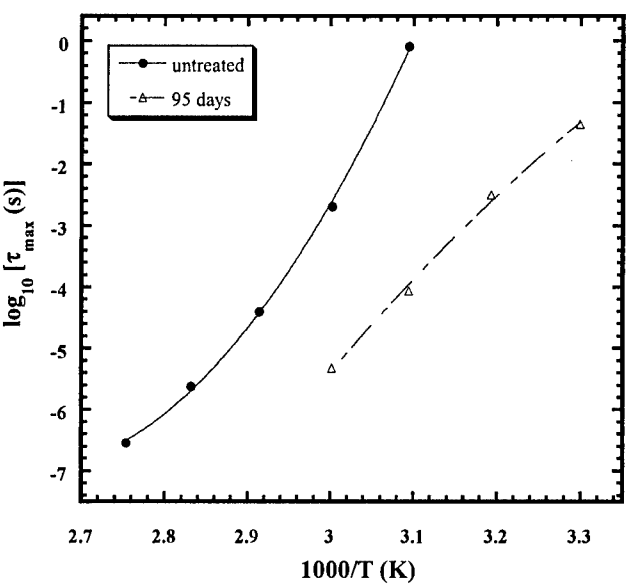

Figure 4. VFTH plot for dry untreated and 95 d degraded samples with the dc conductivity contribution subtracted from spectra.

Other parameters extracted from the HN equation, which reflect the width and asymmetry of the relaxation loss peaks, were used to construct the actual relaxation time distribution, $G(\tau)$, at each degradation time, and the results are shown in Figure 4. $G(\tau)$ shows distinct broadening with less curve asymmetry with increasing degradation time (Figure 5), indicating MW degradation into shorter chain lengths and MW distribution broadening with time.

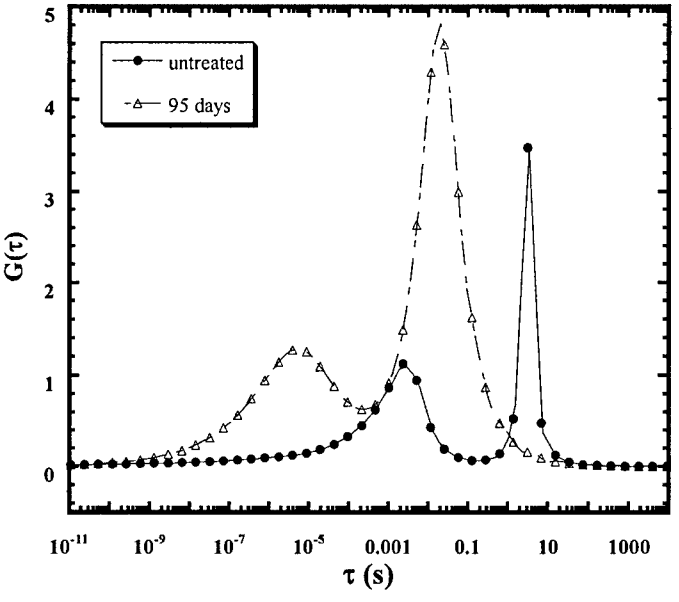

Figure 5. Distribution of dielectric relaxation times at 60° C for dry untreated and 95 d degraded samples.

Both degraded and undegraded samples showed a bimodal distribution but there is distinct curve broadening with less asymmetry for the 95 d degraded sample. This feature is related to the ε" peak asymmetry seen in Figure 5. The unsymmetric distribution is interpreted in terms of molecular weight degradation and molecular weight distribution broadening with time. The shift in curve maximum to lower τ reflects faster chain motions as would be expected of shorter chains.

Similar behavior for the glass transition relaxation peaks of undegraded and degraded 20,000 g/mol PDLLA diacid samples was observed and submitted for publication (2).

These results demonstrate the power of DS in the investigation of biodegradation. This work segment satisfies a pre-stated goal for Year 2 funding.

Hydrolytic degradation of PDLLA containing pendent carboxylic acid groups. To increase degradation rate in seawater we are experimenting with poly(D,L-lactide) (PDLLA) and poly(D,L-lactide-co-glycolide) (PLGA) having carboxylic acid groups regularly spaced along the backbone. Preliminary degradation results for these materials are quite interesting. Figure 6 compares four PDLLA samples as detailed in Table 1. The sample designated BHMBA, containing a single COOH group at the approximate center of the molecule degrades more rapidly (in buffer at 37° C), as expected, than the control sample, D,L-lactide diol, which contains

no carboxylic acid group. It is remarkable, however, that it also appears to degrade more rapidly that the D,L-lactide diacid, which contains a carboxylic acid group at each end of the chain (i.e., 2x the concentration of COOH groups compared to the BHMBA sample). Even faster degradation was achieved by adding more carboxylic acid groups along the chain as shown by the chain extended PDLLA (CE BHMBA) containing an average of 7.3 carboxylic acid groups per molecule.

Table 1. PDLLA Polymers Containing Pendent and Terminal Carboxylic Acid Groups (Degradation data Figure 6)

Sample Designation	Architecture	M_n (g/mol)
BHMBA	HO~~~OH COOH	40,050
CE BHMBA	~~~(~~~COOH)$_{7.4}$	51,150
D,L-lactide Diacid	HOOC~~~COOH	41,810
D,L-lactide Diol	HO~~~OH	41,810

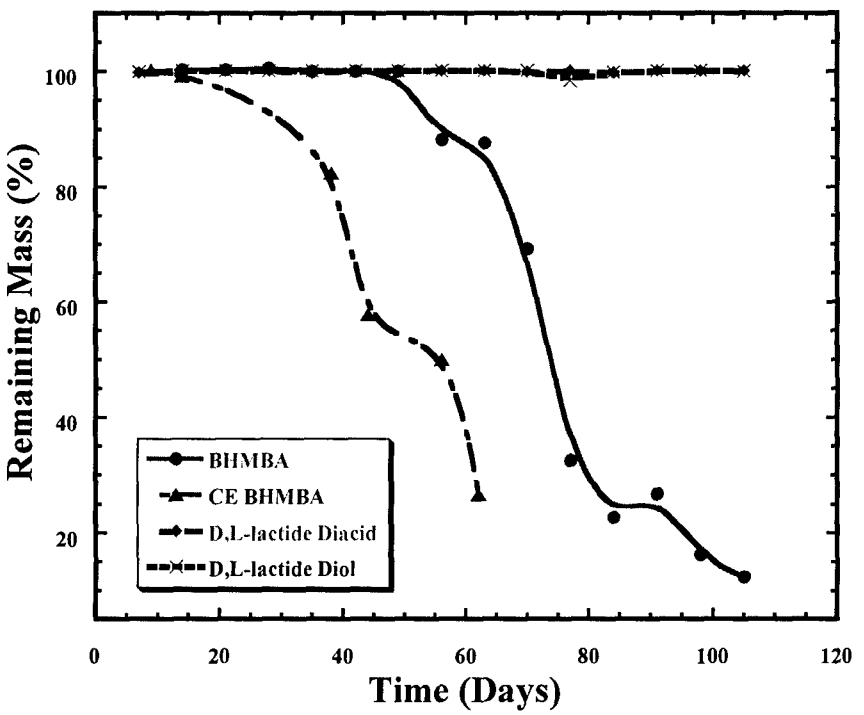

Figure 6. Remaining mass% vs. time for 40K PLA samples containing different numbers of COOH groups along the chain in comparison to diacid and diol terminated samples.

Synthesis and Mechanical Tensile and Dynamic Mechanical Properties Characterization of Degradable Thermoplastic Polyurethanes

Thermoplastic polyurethanes (TPUs) were selected for study since they offer the possibility of incorporating biodegradable polyester chain elements into a family of polymers whose properties can be readily tuned for a variety of applications, including soft plastic and elastomeric applications for which traditional biodegradable polymers are ill-suited. Degradable TPUs were created through the reaction of a diisocyanate with a mixture of a chain-extending diol and a degradable polyester polyol. The product of reaction of the diisocyanate with the chain-extending diol, is termed the hard segment. The relative hard segment content was controlled by the relative amounts of chain extender and polyol and was quantified in terms of the weight of chain extender (1,4-butanediol) times 100% divided by the combined weight of chain extender plus polyol. The -NCO/-OH stoichiometric ratio was held between 1.0-1.1 to account for side reactions that may occur.

The hard segments of the TPUs consist of either L-lysine diisocyanate (LDI)/1,4-butanediol or 4,4'-dicyclohexylmethane diisocyanate (H_{12}MDI)/1,4-butanediol. The soft segments were selected from the following 2000 g/mole polyols: poly(ε-caprolactone) (Dow TONE™ 5249), poly(butylene adipate) (BA, Bayer Desmophen® 2502), poly(D,L-lactide) initiated with 1,4-butanediol (BD-PDLLA), poly(D,L-lactide-*co*-glycolide) initiated with 1,4-butanediol (BD-PLGA), and BA/PLGA mixtures of varying composition. A representative TPU synthesis is pictured Scheme 2.

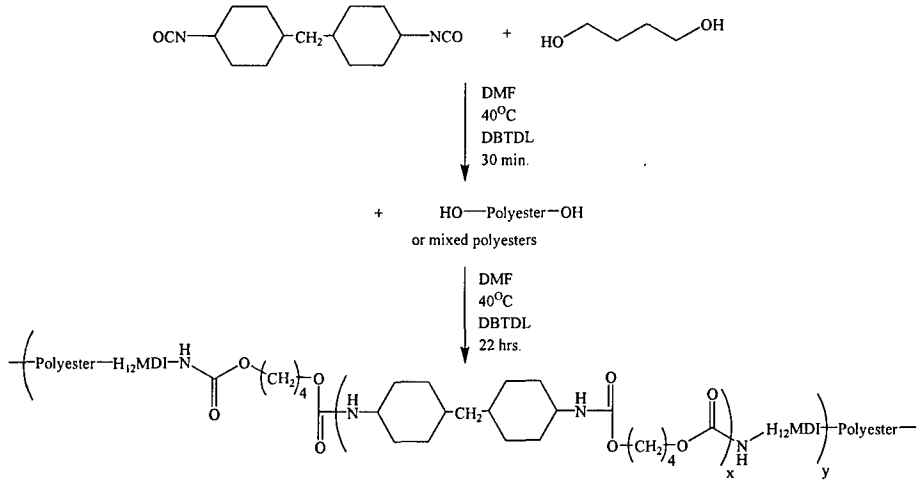

Scheme 2. Synthesis of H_{12}MDI-based thermoplastic polyurethane.

Table 2 lists the polyol compositions of the TPUs synthesized as well as relative molecular weights as compared to PMMA standards. The H_{12}MDI-based TPUs are not soluble in common GPC solvents such as THF, therefore HFIP-GPC was used. TPUs containing PLGA were generally of lower molecular weight. The causes for this are currently under investigation.

Table 2. H_{12}MDI-based TPUs containing 12% hard block (HB) unless otherwise noted.

Polyol Composition	HFIP GPC		
	Mn (g/mol)	Mw (g/mol)	PDI
100% TONE 5249 (LDI)			
100% D,L-Lactide (LDI)			
100%TONE 5249	43,007	202,251	4.44
100% BD-PLGA	7,781	19,881	2.56
50% TONE 5249 50% BD-PLGA	12,455	35,636	2.86
100% BA	51,256	118,975	2.32
50% BA 50% BD-PLGA	12,627	46,121	3.65
75% BA 25% BD-PLGA	10,595	48,951	4.62
6% HB 100% BA	39,304	87,563	2.23
18% HB 100% BA	38,173	85,802	2.25

Tensile stress-strain profiles for TPUs with different soft blocks demonstrate our control of mechanical behavior. Properties range from a very rigid, relatively brittle poly(D,L lactide)-based TPU to tough, elastomeric materials including poly(□-caprolactone) (Tone)- and BA-based TPUs (Figure 7). All the TPUs in Figure 7 possessed a LDI-BD or H_{12}MDI-BD hard segment at 12% relative content. A typical linear low-density polyethylene (LLDPE) stretch wrap film was included in Figure 7 for comparison.

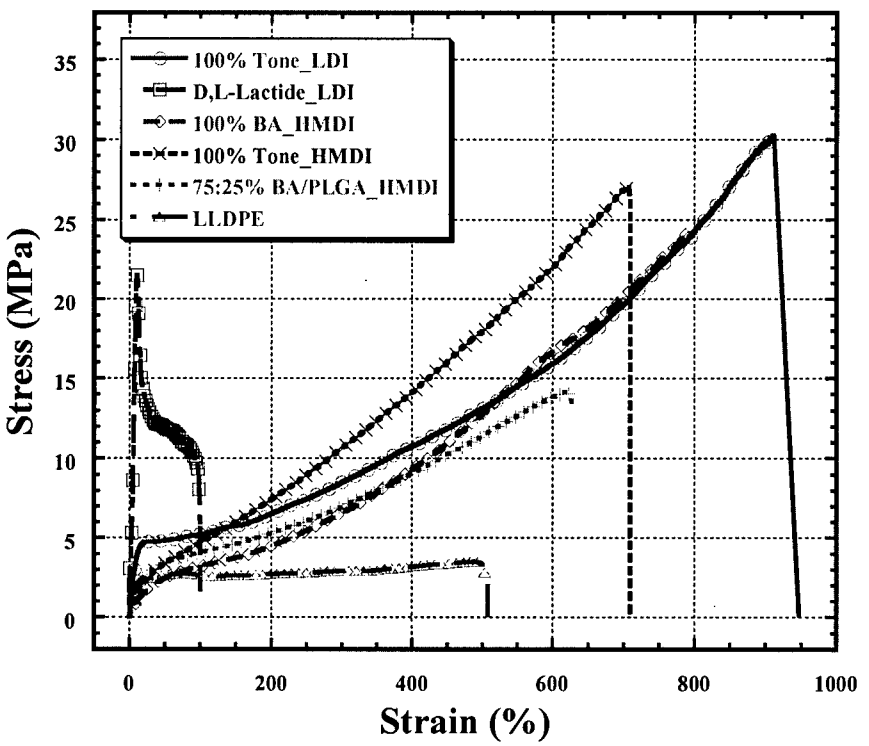

Figure 7. Stress-strain curves of TPUs with 12% HS and different soft segments (SS) compared to a LLDPE stretch wrap film.

Dynamic mechanical analysis (DMA) was used to probe the thermomechanical properties

of the TPUs. Figure 8 shows loss tangent (tan □ vs. temperature curves for BD-LDI or BD-H_{12}MDI-based TPUs at 12% HS, with different polyol soft segments. All TPUs exhibit a sub ambient glass transition temperature (T_g) attributed to the respective soft segments. The Tone-LDI TPU was the only sample to show a distinct T_g attributed to the hard segment (3). The LDI-based TPUs displayed lower melting transitions (T_m) compared to H_{12}MDI-based TPUs, as indicated by a rapid increase in tan □ at about 50-55° C. The highest T_m was achieved with the BA-H_{12}MDI and BA/PLGA- H_{12}MDI TPUs. The best thermomechanical properties were achieved with the combination of H_{12}MDI and BA since both the Tone-H_{12}MDI and the BA-LDI TPUs yielded only small increases in T_m when compared to the Tone-LDI TPU.

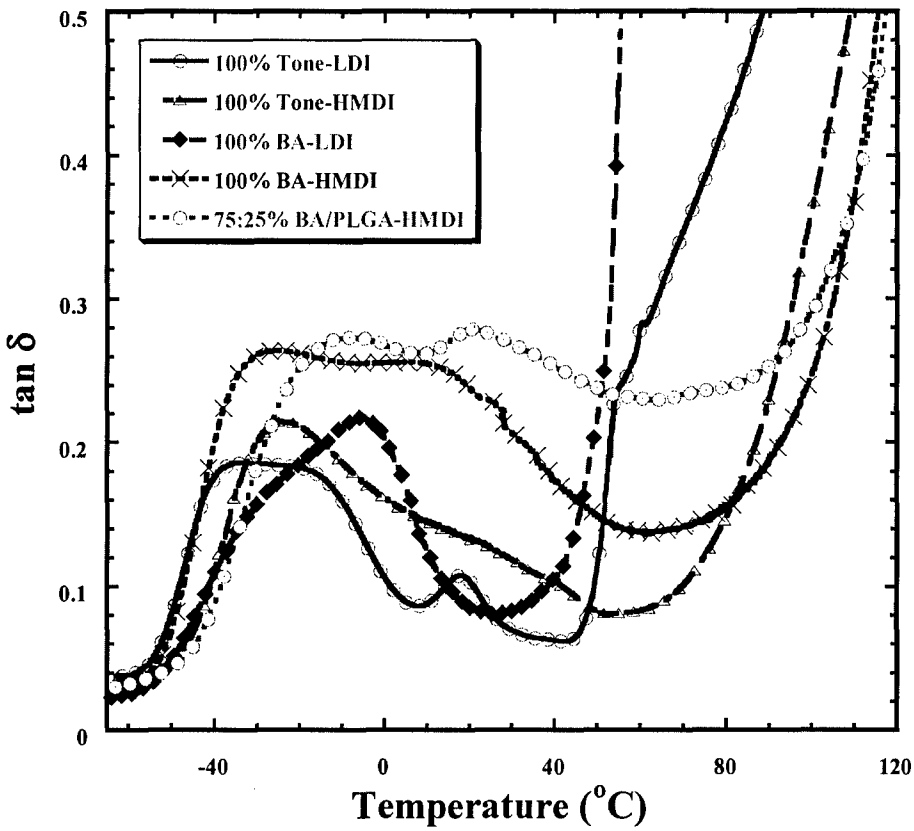

Figure 8. Dynamic mechanical loss tangent of LDI- and HMDI-based TPUs.

While previous work with LDI-TPUs demonstrated good mechanical properties (3), the H_{12}MDI TPUs offer similar mechanical properties along with an improved useful temperature range, which is a significant result.

Comparing data from the LDI-based TPUs (Figure 8) to the curves in Figure 9, it is seen that there is an increase in the onset of melting from 45° C in the LDI system to 63° C in the H_{12}MDI formulation using the same Tone polyol. Replacing the Tone polyol with BA leads to even higher melting temperatures at 83° C. The TPU formulations that include PLGA have increased melting temperatures beyond the 100% BA TPU. These relatively high melting temperatures suggest that these materials would be suited for use at temperatures up to 80-90° C. This is a significant improvement over the LDI-based TPUs previously studied. Also, with the exception of the 50/50 BA/ PLGA polyol-based TPU, the onset of the glass transition remains

well below 0° C, which is typical of an elastomer. The overall useful temperature range for the BA or BA/ PLGA based TPUs is from about -40° C up to 80-90° C.

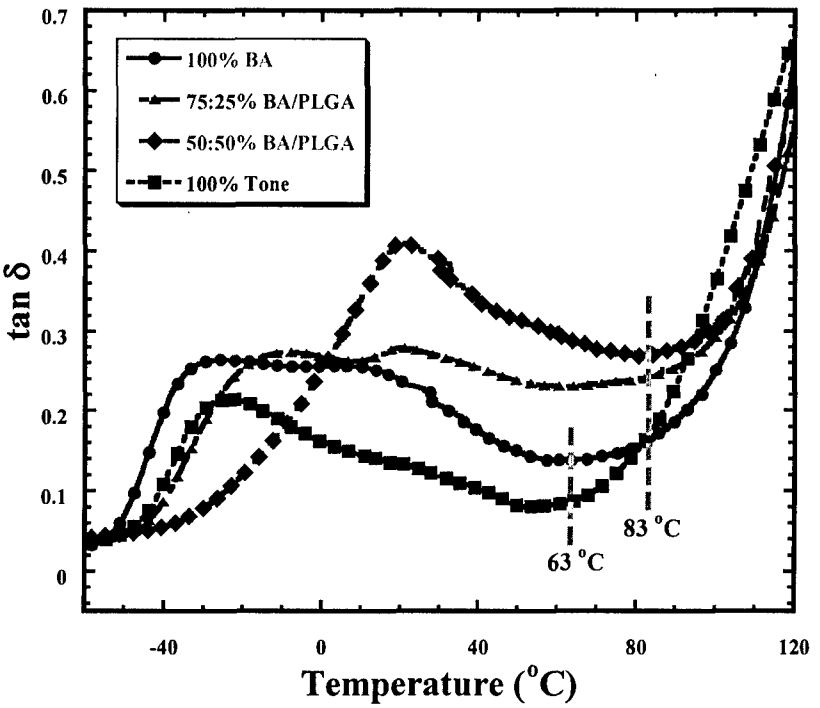

Figure 9. Dynamic mechanical loss tangent vs. T for H_{12}MDI-based TPUs with 12% HS and different polyols. Melting transitions are labeled for 100% TONE (63° C) and 100% BA (83° C).

The mechanical stress-strain curves in Figure 10 indicate good tensile strength, high elongation and excellent toughness. With exception of the 50/50 BA/ PLGA polyol-based TPU, elongations are in excess of 600% and the tensile strengths are above 7 MPa. A LLDPE stretch wrap film was included in Figure 10 for comparison. It is apparent that adding the degradation-enhancing PLGA to the TPU does diminish mechanical properties when compared to the 100% BA-based TPU. However, the properties remain very good especially when compared to other materials such as LLDPE.

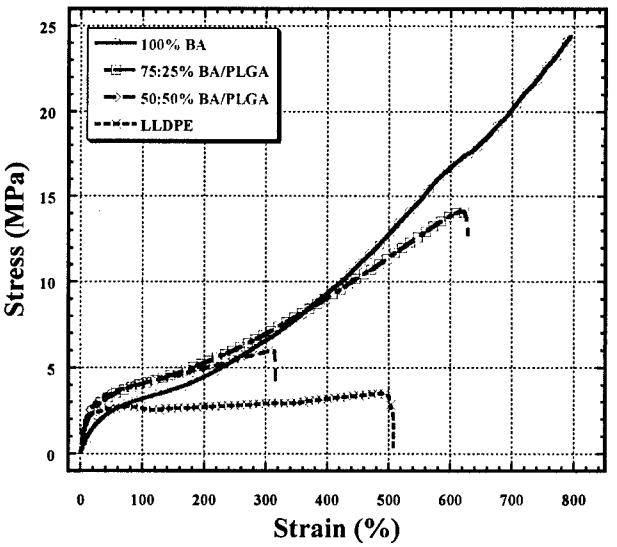

Figure 10. Stress-strain curves of TPUs with different polyol soft segments compared to LLDPE stretch wrap film.

The TGA profile for TPU shows resistance to thermal degradation up to ~ 250° C.

Degradation Studies of TPUs. Previous work showed that PLGA polyols are readily degradable in pH7.4 buffer solution and in the marine environment of the Gulf of Mexico (4). Even more rapid degradation in buffer solution was observed when PLGA was initiated with *bis*-hydroxylmethylbutyric acid (BHMBA) which contains pendant carboxylic acid functionality (4). Based on these observations, it is anticipated that the same trend of enhanced degradation with BHMBA would also occur in the marine environment. Degradation studies of the TPUs in buffer solution are currently underway in the same manner as described previously (5). An early indicator of water uptake is a change in the sample opacity from clear to opaque. This change is evident in the TPU formulations containing PLGA while the TPUs that do not contain PLGA have not yet shown this change. Complete results, including salt water degradation, are forthcoming.

Summary

Degradable TPUs have the potential to become an important class of polymers with commercial and military applications. It was demonstrated that with careful selection of starting materials, TPUs can be customized within a wide range of physical and thermal properties. In addition to excellent properties, there is the environmental benefit of engineering degradable materials. Previous degradation studies of polyester polyols demonstrated the potential of these systems (5). Also, materials based on chemicals present in the human body, such as LDI and lactic acid, have built-in biocompatibility and therefore may potentially be useful in biomedical applications.

Finally, development of such degradable materials that offer good mechanical properties over a wide temperature range will enable the use of degradable materials over traditionally non-degradable ones.

This work represents part of our effort to elucidate structure-property relationships for biodegradable polyesters and poly(ester-urethane)s in a pre-screening program to identify the best material candidates that will be sent to Natick investigators for more sophisticated

evaluations.

References

(1) Hassan, M.K.; Wiggins, J.S.; Storey, R.F.; Mauritz, K.A., "Broadband Dielectric Spectroscopic Characterization of the Hydrolytic Degradation of Hydroxyl-terminated Poly(D,L-Lactide) Materials," *ACS Symp. Ser.* (Polymers for Biomedical Applications) **2006**, in press.

(2) Hassan, M.K.; Wiggins, J.S.; Storey, R.F.; Mauritz, K.A., "Broadband Dielectric Spectroscopic Characterization of the Hydrolytic Degradation of Carboxylic Acid-terminated Poly(D,L-Lactide) Materials," in preparation.

(3) Hassan, M.K.; Mauritz, K.A.; Storey, R.F.; Wiggins, J.S., "Biodegradable Aliphatic Thermoplastic Polyurethane Based on Poly(□-caprolactone) and L-Lysine Diisocyanate," *J. Polym. Sci.: Part A: Polym. Chem.* **2006**, *44*, 2990-3000.

(4) Hassan, M.K.; Mauritz, K.A.; Wiggins, J.S.; Moravek, S.J.; Cooper, T.R.; Storey, R.F. in preparation.

(5) Wiggins, J.S.; Hassan, M.K.; Mauritz, K.A.; Storey, R.F., "Hydrolytic Degradation of Poly(D,L-lactide) as a Function of End Group: Carboxylic Acid vs. Hydroxyl," *Polymer* **2006**, *47*, 1960-1969.

Publications and Presentations

(1) Hassan, M.K.; Mauritz, K.A.; Storey, R.F.; Wiggins, J.S., "Biodegradable Aliphatic Thermoplastic Polyurethane Based on Poly(□-caprolactone) and L-Lysine Diisocyanate, *J. Polym. Sci.: Part A: Polym. Chem.* **2006**, *44*, 2990-3000.

(2) Wiggins, J.S.; Hassan, M.K.; Mauritz, K.A.; Storey, R.F., "Hydrolytic Degradation of Poly(D,L-lactide) as a Function of End Group: Carboxylic Acid vs. Hydroxyl," *Polymer* **2006**, *47*, 1960-1969.

(3) Hassan, M.K.; Wiggins, J.S.; Storey, R.F.; Mauritz, K.A., "Broadband Dielectric Spectroscopic Characterization of the Hydrolytic Degradation of Hydroxyl-terminated Poly(D,L-Lactide) Materials," *ACS Symp. Ser.* (Polymers for Biomedical Applications) **2006**, in press.

(4) Hassan, M.K.; Wiggins, J.S.; Mauritz, K.A.; Storey, R.F., "L-Lysine Diisocyanate Based Biodegradable Thermoplastic Polyurethanes with Broad Range of Mechanical Properties," *ACS Div. Polym. Mat. Sci. Eng.* **2006**, *95*, 656.

(5) Hassan, M.K.; Wiggins, J.S.; Storey, R.F.; Mauritz, K.A., "Novel Method for Characterization of Poly(D,L-lactide) Degradation Based on Dielectric Spectroscopy," *ACS Div. Polym. Mat. Sci. Eng.* **2006**, *95*, 900.

(6) Hassan, M.K.; Wiggins, J.S.; Storey, R.F.; Mauritz, K.A., "Broadband Dielectric Spectroscopic Characterization of the Hydrolytic Degradation of Carboxylic Acid-terminated Poly(D,L-Lactide) Materials," in preparation.

(7) Hassan, M.K.; Wiggins, J.S.; Storey, R.F.; Mauritz, K.A., "Mechanical and Viscoelastic Properties of Biodegradable Aliphatic Thermoplastic Polyurethane Based on Poly(ε-caprolactone) and L-lysine Diisocyanate," in preparation.

Poster Presentations

(1) Hassan, M.K.; Wiggins, J.S.; Mauritz, K.A.; Storey, R.F., "L-Lysine Diisocyanate Based Biodegradable Thermoplastic Polyurethanes with Broad Range of Mechanical Properties," ACS Fall 2006 Meeting, San Francisco, CA.

Oral Presentations

(1) Hassan, M.K.; Wiggins, J.S.; Storey, R.F.; Mauritz, K.A., "Novel Method for Characterization of Poly(D,L-lactide) Degradation Based on Dielectric Spectroscopy," Polymers for Biomedical Applications Symposium, ACS Fall 2006 Meeting, San Francisco, CA.

Novel Biodegradable Films Based on Cross-linked Dendritic Aliphatic Polyesters Containing Multiple Functional Hydroxyl Groups

Personnel

The focus of this research program has been directed towards the fundamental understanding and optimization of structure property relationships of novel biodegradable, hydroxylated dendritic aliphatic polyesters and their networks prepared via cross-linking with different diisocyanates. This activity was directed by Assistant Professor S. Nazarenko (Department of Polymer Science at USM). The participating in the project lab personnel included post-doctoral associates Dr. Brian Olson (NazRG) and Dr. Grace Chigwada (NazRG), and also a graduate student Jason Pratt (NazRG). The work was conducted in collaboration with the groups of Profs. Wicks, Rawlins, Storey, Mauritz, and Wiggins.

Summary

Dendritic polymers possess unusual structures and exhibit properties that differ dramatically from those of the more traditional polymer types. These features have contributed to multi-disciplinary applications of these polymers. The development of efficient synthetic routes in recent years made some of the dendritic polymers commercially available in unlimited quantity, and at very affordable price.

This report reflects on a novel approach of making biodegradable, flexible, transparent, high oxygen barrier films based on polyhydroxylated dendritic polyols crosslinked by linear aliphatic, 1,6-hexamethylene diisocyanate (HDI).

The scope of this report encompasses aspects of synthesis, fundamental understanding and optimization of the cross-linking reactions, mechanical and gas barrier, as well as biodegradation behavior.

Current Approach

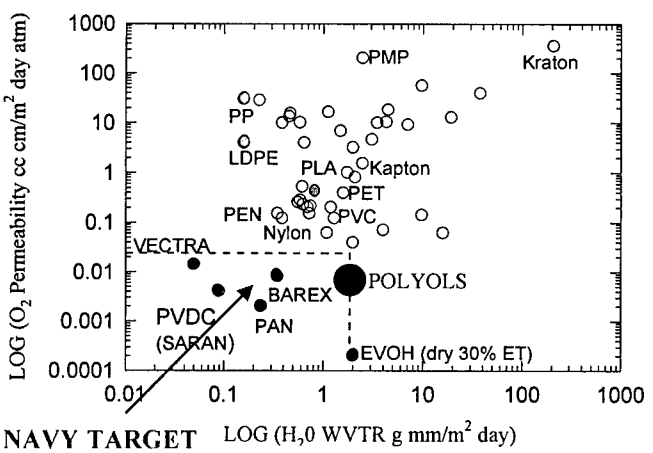

Fig 1 Oxygen permeability versus vapor transmission rate for various polymers

Biodegradability is promoted by enzymes and may be either aerobic or anaerobic. It is generally accepted that only some hetero-chain polymers, i.e., aliphatic polyesters are truly biodegradable, although in practice the bio-assimilation step is normally preceded by abiotic hydrolysis which results in monomeric and oligomeric products that are more readily consumed by microorganisms that are present. To our best knowledge, none of the commercially available biodegradable aliphatic polyesters so far considered for packaging applications exhibit an oxygen barrier that is high enough to satisfy the barrier constraints for packaging oxygen-sensitive

food. Fig. 1 shows oxygen permeability versus water vapor transmission rate (WVTR) for various rubbery and glassy polymers, including PLA-poly(lactic acid) which is a typical commercial biodegradable polyester. Other biodegradable polyesters such as PGA-poly(glycolic acid), PCL-polycaprolactone and PHBV-poly(3-hydroxybutyrate-co-3-hydroxyvalerate exhibit oxygen barrier properties similar to that of PLA. While most commercially available biodegradable polyesters are reasonably good water barriers, their oxygen barrier property is fairly marginal. So, for the packaging of oxygen sensitive foods, their application is limited. In turn, a few commercially available high oxygen barrier polymers such as PAN-poly(acrylonitrile), PVDC -poly (vinylidine chloride), thermoplastic liquid crystalline Vectra, and EVOH, are not biodegradable.

In particular, hydroxyl-functionalized polymers have a potential to exhibit good gas barrier properties. For instance, changes of the molar content of vinyl alcohol groups in EVOH polymer, one of the typical high oxygen barrier polymer, from 20 to 80 % lead to nearly four orders-of- magnitude change in oxygen permeability. In short, the effect of hydrogen bonding on gas barrier is dramatic. Inspired by this analysis, we turned our attention towards inexpensive dendritic hydroxyl functional hyperbranched polyesters based on 2,2-bis-methylopropionic acid (bis-MPA) with an ethoxylated pentaerytriol (PP50) core available from Perstorp Specialty Chemicals AB, Sweden (trade name Boltorn^{TM})[4] expecting not only a high oxygen barrier, which is essential for various packaging applications, but also biodegradability because these structures represent generally biodegradable aliphatic esters in contrast to EVOH. Figure 2 shows the structure of fourth (H40) generations of Boltorn^{TM} containing multiple functional hydroxyl groups, 16(H20), 64 (H40). The pseudo-one-step, divergent synthesis of these aliphatic- ester hyperbranched polymers, first described by E. Malmström *et al.* in 1995, involves sequential addition of monomer during synthesis; each addition corresponds to the stoichiometric amount of the next theoretical generation. Although characterized by imperfect branching and significant polydispersity, these polymeric structures preserve the essential features of dendrimers, namely, high end-group functionality and a globular architecture. Experiments showed that indeed compression molded films prepared from these polymers exhibited superb oxygen barrier properties, and natural brittleness of these can be dramatically improved via cross-linking with diisocyanates with practically no sacrifice of oxygen barrier.

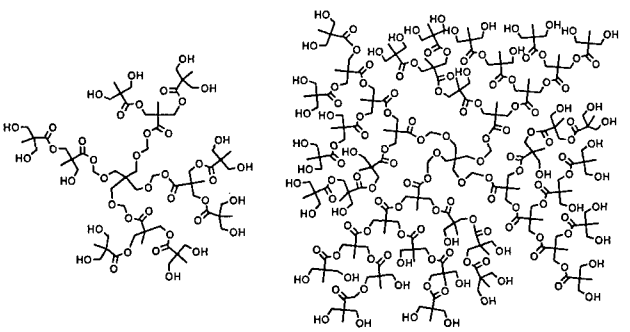

Fig2 Representative structure of Boltorn™ polyols of generation 2 and 4.

Cross-linking Reactions Protocol

Last year efforts were focused on preparation and investigation of polyol system cross-linked

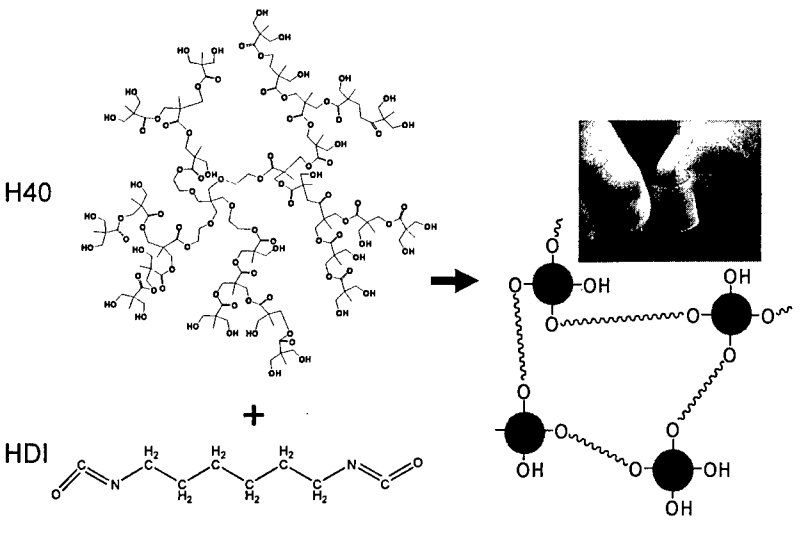

Fig3 Schematics of cross-linking reactions

with flexible aliphatic diisocyanate 1,6-hexamethylene diisocyanate (HDI). The schematics of cross-linking of Boltorn^{TM} H40 with HDI is shown in Figure 3. Prior to cross-linking, H40 polyol pellets was carefully dried in a vacuum chamber at 110°C for 24hrs. A 250 ml round bottom flask and stir bar were dried at 90°C and then 3g of the dried H40 polyol was added. The round bottom flask with H40 was placed into a silicon oil bath heated to 130°C under N_2 purge to remove any residual moisture that may have been absorbed during handling. Then, the flask was capped with a water jacketed condenser to prevent any solvent from evaporating from the system. N,N- dimethylformamide (DMF) of 99.8% of purity was added to the reaction vessel through the condenser septum and the N_2 purge was further continued followed by cooling the system down to desired temperature, about 90°C, at which the cross-linking reaction was carried out. For each cross-linking composition (NCO/OH ratio), the reaction temperature has been specifically optimized, so the characteristic time before gelation was about one hour. The kinetics of the reaction was also studied using FTIR. Once the proper reaction temperature was set, the predetermined amount of HDI was added to the system. The amount of HDI added for a given NCO/OH ratio, and the temperature of the reaction is shown in Table 1. The continuous N_2 purge was stopped and replaced with an N_2 filled balloon to maintain positive pressure on the system thus preventing any moisture from entering the reaction vessel. Observation of the reaction vessel was maintained over the course of the reaction to monitor the viscosity of the solution. As the viscosity increased to the level, so the reaction was nearby the gelation point, the solution was cast onto glass plate and left in the fume hood for 12 hrs to

Table 1

%NCO/OH	g HDI per 100 g H40	Reaction temperature (°C)	Reaction time (min)
0	0	90	60
5	5	90	60
7	7.3	90	60
10	10.3	90	60
15	16	90	60
20	21	90	60
25	26	90	60
30	31	90	55
35	36	90	55
40	42	90	55
45	47	90	50
50	53	80	60
60	63	80	60
70	74	80	60
80	84	70	65

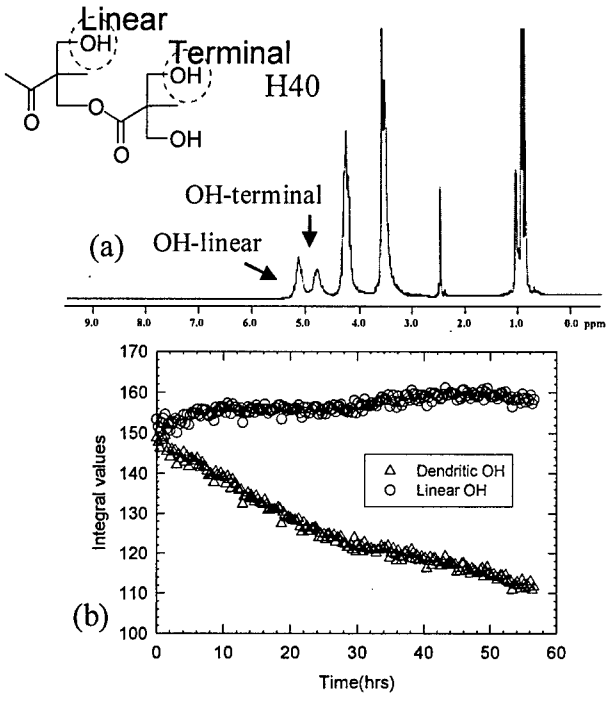

Fig4. (a)^{1}H NMR of Boltorn^{TM} in DMF at RT; (b) The kinetics of consumption of terminal and linear OH groups of H40 upon reaction with HDI at RT;

evaporate the residual DMF. The resulting film (~0.1 mm thick) was then peeled and further dried in a vacuum chamber for 72 hrs at 55°C. Finally, all samples were annealed at 155°C for one hour in vacuum in order to remove any remaining traces of DMF solvent as the boiling temperature of DMF at 1 atm pressure is 142°C. The physical properties of free of solvent samples were measured. 70% and 80% cross-linked films were attempted but were severely opaque (blushed) due to the formation of urea because the increased sensitivity to ambient moisture with increased isocyanate concentration.

Probing the Cross-linking Reactions Mechanism by ^{1}H NMR

Because H40 is not a perfect dendrimer, not all the hydroxyl groups are terminal, about 50-60% of them are situated in the linear segments of internal dendritic structure leading to the degree of branching of these systems about 40-50%. Therefore the question can be posed whether there is a difference in reactivity between terminal dendritic and linear hydroxyl groups. ^{1}H NMR (500 MHz Bruker) allows a direct monitoring of the consumption of these groups upon cross-linking via monitoring the changes of area under corresponding peaks representing linear and dendritic (terminal) hydroxyl groups. The characteristic NMR spectra of H40 showing these two peaks is displayed in Figure 4a). The experiments conducted at various temperatures (very slow one, carried out at RT, is shown in Fig 4b), revealed that the terminal hydroxyl groups react with isocyanate groups much faster in comparison with linear OH groups. Linear OH groups, which can be envisioned as to be hidden inside the dendritic structure are "screened" by the neighboring atoms and therefore are much less reactive. So, the cross-linking of H40 with HDI occurs primarily via reaction of isocyanate groups with the peripheral hydroxyl groups.

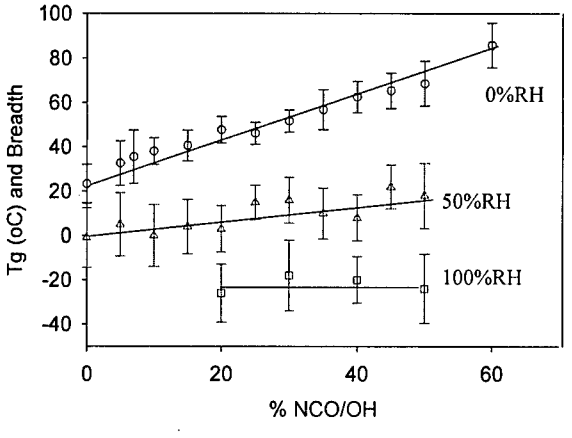

Fig 5. Tg of Cross-linked systems as a Function of NCO/OH ratio and 0, 50 and 100% of relative humidity

Studying of Tg and Rubbery Elasticity Plateau Modulus of Cross-linked Systems

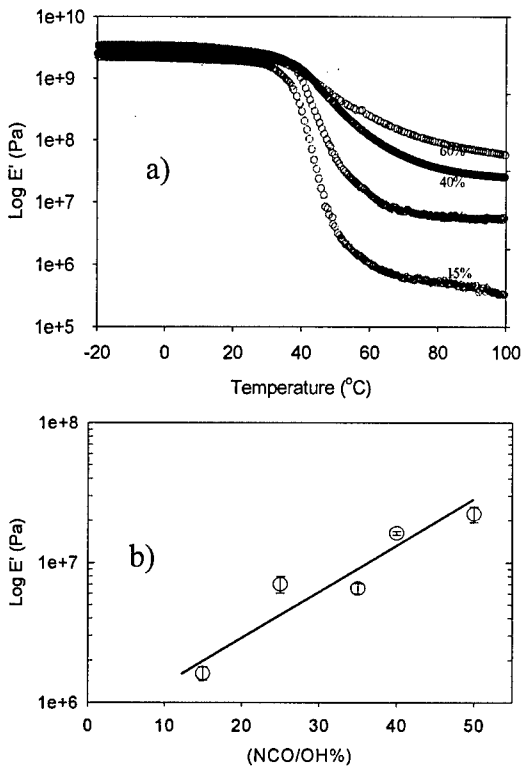

Fig6. (a) DMTA (LogE' versus T) curves for cross-linked systems characterized by different NCO/OH; (b) LogE' as a function of NCO/OH ratio;

The second question was posed whether cross-linking is predominantly inter-molecular or intra-molecular. Dendritic polymers represent multivalent scaffolds, so the possibility that one HDI molecule reacts with two hydroxyl groups of the same dendritic unit can not be ruled out. Intra-molecular cross-links, associated with formation of loops, are not as efficient as inter-molecular cross-links, and typically lead to leveling off the glass transition temperature and rubber elasticity plateau modulus. To explore this behavior the dependencies of Tg and LogE' versus NCO/OH ratio were measured. Fig5 shows the glass-transition temperature versus NCO/OH ratio representing the ultimate degree of cross-linking. The Tg was determined by DSC at 0, 50, and 100% of relative humidity. Tg at 0%RH were determined from second scans, first scans were used to determine Tg at 50 and 100%RH for samples specifically conditioned at these levels of relative humidity prior testing. The observed gradual increase of Tg as a function of NCO/OH ratio observed at 0%RH is in agreement with the predominant formation of intermolecular cross-links. Tg gradually increased from about 20°C to 90°C by changing NCO/OH ratio from 0 to 60%. Humidity obviously plays a pivotal role in lowering Tg due to breaking of the existing hydrogen bonding network and plasticizing the network structure. Fig 6a shows DMTA data, i.e. Log E' versus temperature for cross-linked samples. As anticipated Tg is increased with the increase of NCO/OH ratio. Moreover, rubber elasticity plateau also increases with NCO/OH ratio (Fig6b), in agreement that cross-linking of Boltorn™ with HDI is predominantly associated with the formation of inter-molecular cross-linking.

Large Strain Deformation Behavior of Cross-linked Boltorn™ Polyols

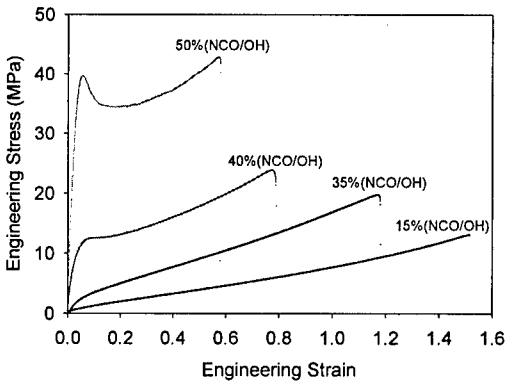

Fig7 Stress-strain behavior of Boltorn™ cross-linked with HDI

All cross-linking materials showed dramatic improvement of mechanical properties at ambient conditions. It was possible to obtain stiff, very flexible films with elongation at break as large as 150% (Fig 7). Previously we reported even larger values of elongation at break. But those samples were apparently slightly plasticized with the residuals of DMF solvents. Extra precaution measures incorporated this year, such as drying in the vacuum above boiling temperature of DMF permitted to obtain more realistic numbers. As one can see from Fig7, the cross-linked materials become stiffer with the increase of NCO/OH ratio. The elongation at break, naturally, shows an opposite trend.

Biodegradation of Pure Boltorn™ polyols and Preliminary Investigation of Abiotic Degradation of the Cross-linked System.

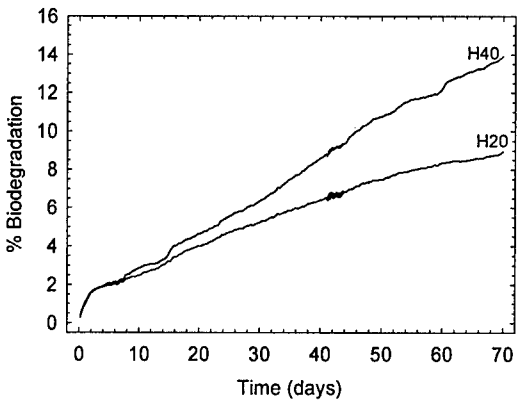

Fig 8. Biodegradation behavior of pure polyols.

Because Boltorn™ dendritic polyols represent the class of aliphatic esters, they are potentially biodegradable. Biodegradation behavior of pristine Boltorn™ dendritic polyols is illustrated in Fig8. The tests were conducted at Natick in collaboration with Dr. J-A. Ratto. The samples were subjected to a specific blend of aqueous bacteria and the byproducts of degradation were measured via gas chromatography. The percent biodegradation was defined according to ASTM D5338 from the amount of CO_2 released. Fourth generation dendritic polyols lost 14% of their total carbon content in as little as 70 days. Assuming similar trend is continued, by 280 days as much as 56% is expected to assimilate. The gradual loss of carbon appears to be associated with a surface biodegradation mechanism. So, if the process was associated with bulk degradation behavior, naturally the rate of biodegradation would be considerably expedited. The difference between 2nd and 4th generation's biodegradation behavior can be

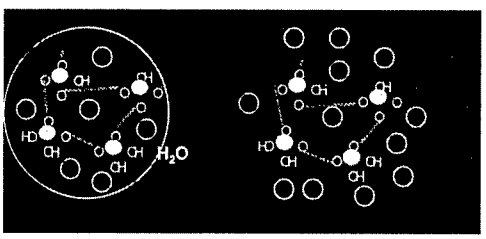

Fig9 "Inflation" model for abiotic degradation of cross-linked Boltorn™

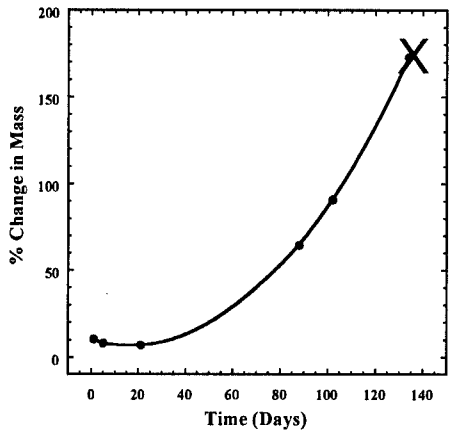

Fig10. Mass uptake curves of cross-linked with HDI Boltorn™ dendritic polyols with NCO/OH=35%

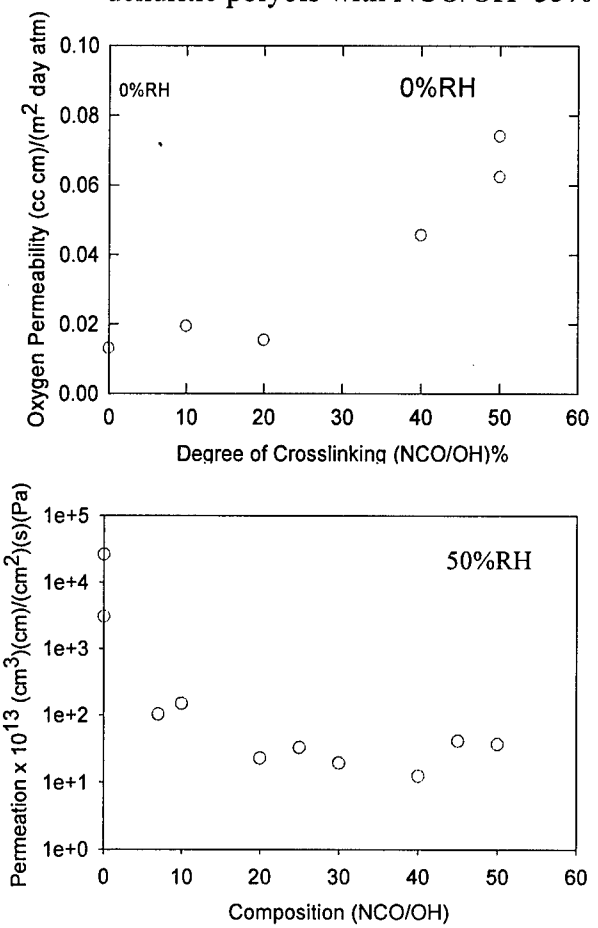

Fig11. Oxygen at 0%RH and water at 50%RH permeability of cross-linked Boltorn™ polyols

attributed to the difference in the volume fractions of aliphatic ester groups. Evidently, 4th generation is characterized by larger volume fraction of aliphatic ester groups as compared to 2nd generation. Several cross-linked systems are currently on the way to Natick for a direct biodegradation testing. In the mean time, we investigated abiotic (associated with hydrolysis reactions) degradation behavior of pure H40 and the cross-linked system with NCO/OH =35%. The film samples under comparison were placed in the buffer aqueous solution at 37°C while their weight was periodically measured. The interesting feature of cross-linked samples as compared to pure H40 is that they easily form a hydrogel in the buffer solution while H40 remains essentially unswelled (Fig 9). Moreover, it was observed that the size of swelled cross-linked samples was exponentially increasing with time indicative of the decreased cross-linking density due to the hydrolysis reaction in the bulk. The "inflation" model illustrating this behavior is shown in Fig 9. Eventually, highly swelled cross-link sample completely disintegrated practically over night ("exploded") after being exposed to the aqueous environment for about 5 months. The mass uptake kinetics of the cross-linked sample is shown in Fig 10 with the cross indicating the point at which the sample disintegrated completely. Interestingly, that the sample of pure H40 degraded in aqueous environment much slower as compared to the cross-linked one. The difference in the rate of abiotic degradation was attributed to the fact that cross-linked samples degrade via bulk-degradation mechanism while pure H40 degrade via surface degradation mechanism which is apparently slower than the bulk one.

Oxygen and Water Barrier of Cross-linked Boltorn™

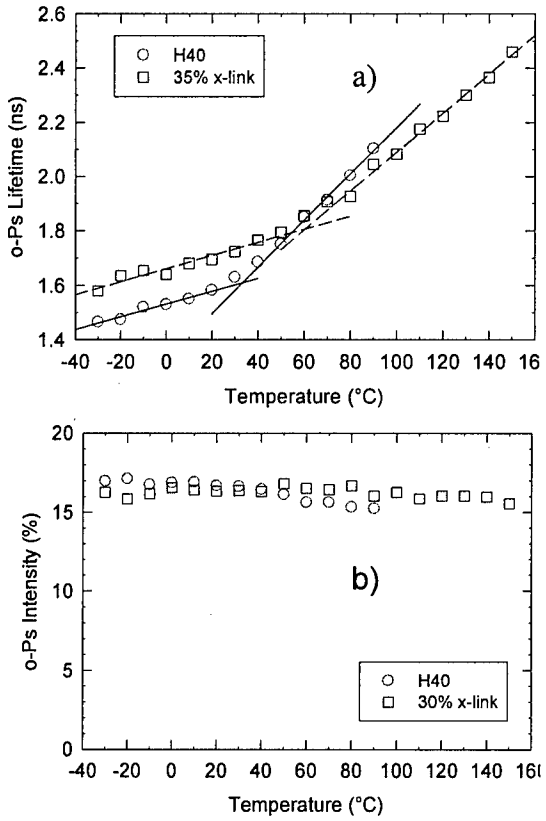

Fig12. Positron annihilation assessment of free volume behavior of pure H40 and H40 cross-linked with HDI (a)life-time behavior; (b) Intensity behavior

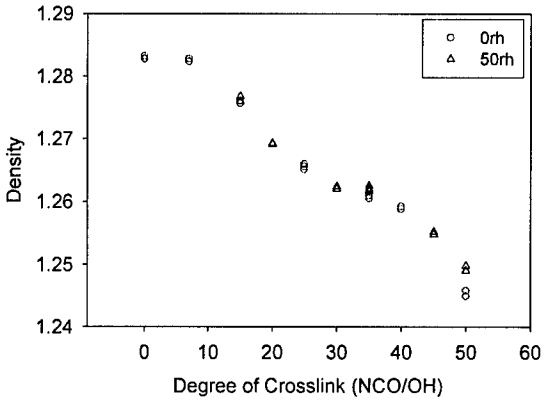

Fig.13 Density behavior of cross-linked Boltorn™ polyols

Primarily because of multiple hydroxyl groups in the structure of Boltorn ™ polyols, these dendritic polymers exhibit excellent gas barrier comparable with that for EVOH with about 50mol% of ethylene content in the structure. Oxygen barrier (permeability coefficient) at 0% RH and water barrier (permeability coefficient) of cross-linked systems are shown in Figure11 as a function of NCO/OH ratio. The oxygen permeability measured at 0%RH increases (barrier decreases) by about one order of magnitude as the degree of cross-linking (NCO/OH) increases from 0 to 50%. Interestingly, that within practically important range of cross-linking (0-35%) when the films exhibit outstanding mechanical performance, the oxygen barrier of cross-linked systems is not that different from the pristine H40. Oxygen permeability starts increasing strongly only above 30% of cross-linking. The decrease of gas barrier can be attributed in general to two factors. The first factor is associated with the consumption of hydroxyl groups upon cross-linking with HDI. The hydroxyl groups are known to form fairly strong hydrogen bonds. However, upon cross-linking with diisocyanate they are replaced with amine groups which are also capable to form the hydrogen bonds. So, it is unlikely that the first factor dominates in defining the gas barrier behavior. The second factor can be attributed to the increase of free volume due the increase of Tg with cross-linking. Larger free volume naturally must results in larger permeability coefficient. On other hand, the higher Tg, the larger none-equilibrium volume is accumulated upon cooling. Probing free-volume with positron life time spectroscopy (PALS) showed that indeed, cross-linked samples exhibited larger free volume as compared to pure H40 primarily due to the larger size of molecular cavities as judged from the difference of the corresponding life times measured at room temperature (see Fig 12a). The corresponding intensities shown in Fig 12b are about the same for pure H40 and the cross-linked sample. The direct density measurements also showed that density is decreased with the cross-linking in agreement with the direct assessment of free volume by

PALS. Water barrier measured at 50%RH however displayed a quite different trend with cross-linking as compared to oxygen barrier. Water permeability decreased dramatically (several orders of magnitude) for cross-linked samples as compared to pure H40. The explanation of this unusual behavior can be attributed to the increased hydrophobicity of cross-linked samples as well as the possibility that at 50%RH highly cross-linked systems are still in the glassy state while less cross-linked samples including pure H40 are in the rubbery state due to plasticization effect of water (see Fig5). It is known that permeability of a polymer in the glassy state is considerably larger than that in the glassy state. Further measurements of both oxygen and water barrier at various RH are on-going at the moment to address this matter more rigorously.

Evaluation of Film Composition on Biodegradation
Douglas Wicks

Biodegradation of polymeric materials in the environment is a complex process involving concurrent actions of chemical, photochemical and biological attack on the material. The degradation of fabricated materials goes beyond just that of the mainstay polymer it self, it is also greatly influenced by the additional components that are included. These additional components include surfactants, lubricants, dispersants, pigments and thermal/UV stabilizers. Each of these components can affect the degradation of the polymers through either changes in product morphology that allow for improved penetration of water/microbes or they may play chemical role in the decomposition.

Existing methodologies for the evaluation of aerobic biodegradation are too time consuming to be applied to a wide breadth of products and product formulations. ASTM 6691-01 *Standard Test Method for Determining Aerobic Biodegradation of Plastic Materials in the Marine Environment by a Defined Microbial Consortium* is the standard for evaluation within the industry and for the current RFA. The procedures for this test call for a 5 part protocol for evaluating the biodegradability of a polymer. This that takes a minimum of 30 days to get results. [i]

Summary of Results from Second Segment of Project

Polyurethane dispersions were chosen as models for the degradation of polyurethane elastomeric films due to the ease of fabrication of films through casting and because of the large diversity of molecular structures available. Initial screening was performed on polyester (BD Adipate), polycarbonate (HD Carbonate), and polyether (PTMEG) dispersions that had either amino-carboxylate or sodium sulfonate dispersing groups.

Hydrolysis experiments on cast films showed that only the polymers with both the polyester diol and the carboxylate dispersing group degraded appreciably after exposure to salt water for 2 weeks. Similar results were found for supporting microbial growth. This was found to take place regardless of the type of polyester used – all were equally good at encouraging microbial growth. Clearly the polymers have to physically breakdown before being microbial digested.

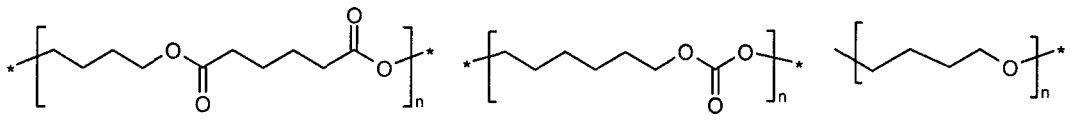

Figure 1. Polyols used in polyurethane preparation – butanediol adipate, hexanediol carbonate and polytetramethylene glycol.

The urethane and urea segments do not hydrolyze under these conditions. The polyester segment is the hydrolytically unstable portion of the urethane (Figure 2). When the films are prepared with a carboxylate salt dispersant such as DMPA (dimethylol propionic acid), the free carboxylic acid is regenerated after film formation due to evaporation of the neutralizing amine. This acid then catalyzes the ester hydrolysis reaction.

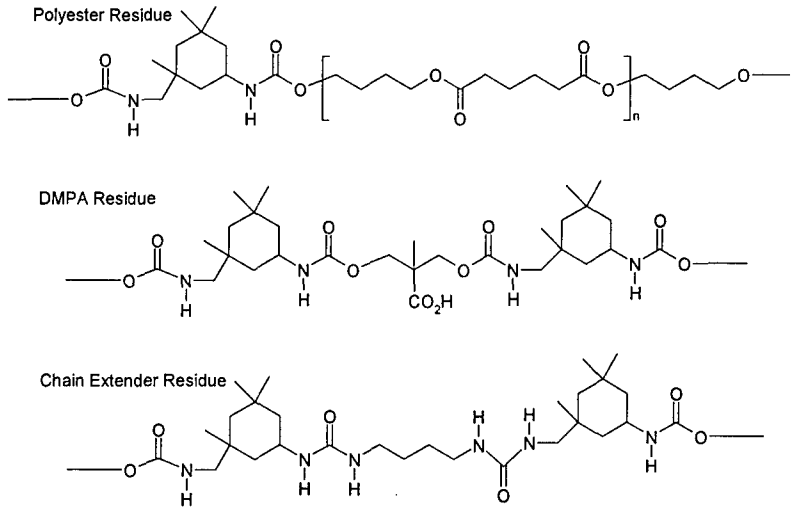

Figure 2. Compositional segments of solid films prepared from polyurethane dispersion

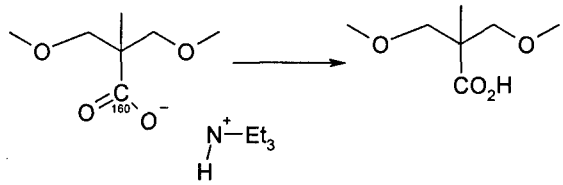

Figure 3. DMPA residues in PU Dispersions forming catalytic carboxylic acid

Experimental

Bacterial viability studies were carried out with a number of organisms. To screen biodigestion of the materials, the following protocol was used: 1. Cast films into glass vials; 2. Incubate films for 2 weeks at 40C in seawater; 3. Inoculate samples with microbe (roughly 7 x 10^3 cfu in 600 microliters) 4. measure microbe population after 48 hrs. If there is an increase in population vs the control biodigestion is assumed to have taken place, a decrease vs the control would indicate that a toxic hydrolysis fragment was released.

Experiments were carried out using a 96-well plate layout. A typical microtiter plate is shown below in Figure 4. Readings for cell population were made using standard fluorescence or optical density measurements that had been calibrated against well characterized standards.

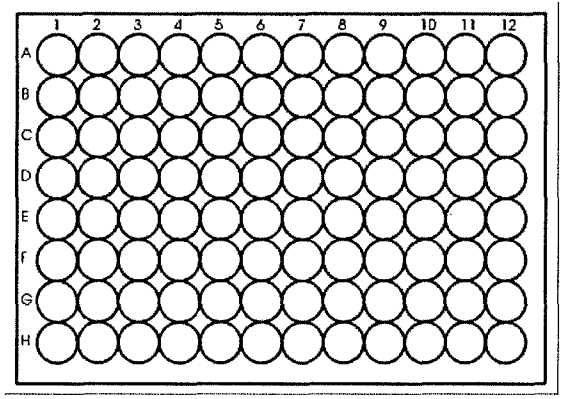

1 Figure 4 microtiter plate layout

Figure 5 shows representative results of the fluorescence spectra obtained after 24 hours of microbe incubation in seawater. On the left is a measurement of a sample without the polymer film present, while on the right were taken with a polyester carboxylate dispersion film. The top measurement was in the presence of added nutrients (TSB).

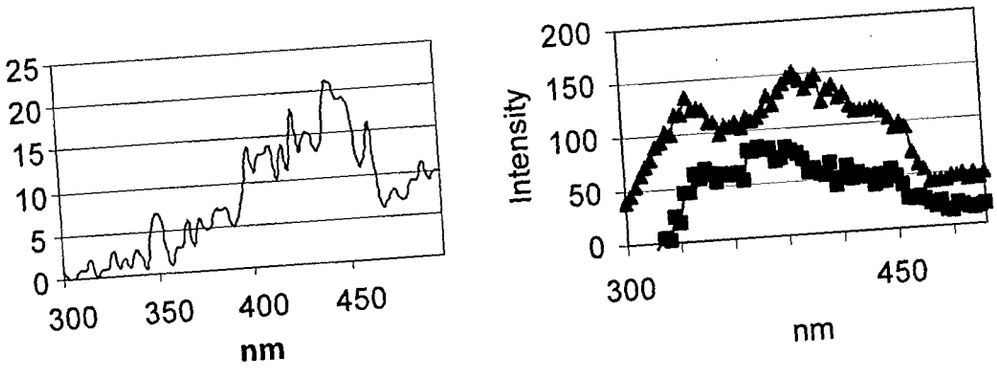

Figure Fluorescence intensity for samples without PUD(left) and with polyester based polyurethane (right, with and without added nutrients).

2006 ONR Annual Report
Lon Mathias

Progress to date

Excellent progress has been made on developing new approaches to nanocomposites and "salt water triggered" dissolution and degradation of polyester composites. We have:

- Prepared nanocomposites based on poly(ε-caprolactone) and organically modified montmorillonite
  - Synthesized a novel imidazolium surfactant having two long alkyl chains one of which contains hydroxyl group as a chain terminal (the product isolated with an excellent yield)
  - Determined the chemical structure of surfactant by NMR spectroscopy
  - Prepared organically modified montmorillonite by ion-exchange reaction between surface bound sodium cations and imidazolium surfactant
  - Determined the amount of organic compound incorporated onto montmorillonite by TGA (the organic content determined as 22 wt-%)
  - Revealed intercalation of surfactant between clay platelets by XRD (d-spacing value of pristine montmorillonite increased from 11.8 Å to 18.0Å upon modification)
  - Prepared nanocomposites by in-situ intercalative polymerization of ε-caprolactone by using hydroxyl functionality of the surfactant to either react with monomer or polymer
  - Prepared a series of nanocomposites with 1 to 5 wt-% organo-montmorillonite loadings (the inorganic content revealed by TGA was in accordance with targeted amounts)
  - Evaluated polymer formation by NMR and FTIR spectroscopy
- Completed characterization of nanocomposites
  - Recovered polymer chains from the surface of clay platelets by reverse ion-exchange reaction with lithium cations in THF fallowed by centrifugation
  - Determined molecular weight of polymer by GPC (the molecular weight of PCL chains was controlled by the terminal hydroxyl content; i.e., by the organo-montmorillonite content)
  - Analyzed morphology of nanocomposites by XRD and TEM (the hydroxyl functionality on long alkyl chains had improved ability for grafting of polymer chains from the surface of the clay verified by the highly exfoliated morphology obtained)
  - Evaluated thermal behavior by DSC as well as TGA measurements (highly exfoliated nanostructure does not affect thermal events such as T_m, T_c, T_g, and T_d, the platelets clearly act as nucleating agents for crystallization of PCL matrix and degree of crystallinity increases with clay content)
  - Revealed mechanical properties by DMA (the storage moduli enchanced particularly above T_g, upon increasing the clay content)

Need

The progress made to date indicates that the new materials and the new conceptual approaches to obtaining dissolvable and degradable polyesters with the desired set of properties is on-track. We have opened up new pathways that offer exciting initial results and that promise

to develop these new materials in an iterative fashion over the next year.

Goals and objectives for 2006-2007

Based on the exploratory and developmental work accomplished this year, we plan on examining several components in depth. These include:

- Preparation of biodegradable polyester nanocomposites with different compositions by utilizing a design-of-experiments protocol
  - Montmorillonite and laponite nanolayers, silica and titania nanoparticles will be used as inorganic reinforcing agents.
  - Modification of inorganic particles will be carried out by using organic cations and silane coupling agents with and without functional groups.
  - Surface modification of layered silicates will be carried out ion-exchange reaction between exchangeable cations and organic surfactants.
  - Hydroxyl groups which are assumed to be on the edge of the clay platelets will be utilized for edge modification.
  - Silane coupling agents will be used for surface modification of silica and titania nanoparticles.
  - The functional groups of the surfactant will be utilized either to initiate the polymerization "grafting from" or to react with the functional groups of the polymer "grafting to".
  - In the case of non-functional surfactants external initiators will be used for in-*situ* polymerization.
  - Control experiments with unmodified nanoparticles will be also carried out.
  - Poly(3-hydroxypropionic acid) homo and copolymers as well as other biodegradable polyesters such as poly(caprolactone) and polylactide will be used for preparation of nanocomposites.
- Evaluation of nanoscale and macroscopic behavior of nanocomposites
  - The formation of polymers will be followed by ^{1}H and ^{13}C NMR spectroscopy as well as by FTIR spectroscopy. The end group analysis of telechelic polymers was performed by means of NMR spectroscopy and standard titrimetric methods. Solid-state ^{13}C and ^{29}Si NMR spectroscopy will be also utilized to determine chemical composition of nanocomposites.
  - XRD will be used for initial characterization of organically modified clay/nanoparticles and nanocomposites. TEM and SEM will allow direct visualization of nanoparticle dispersion throughout the polymer matrix. Crystallization behavior of polymer within the nanocomposite will be investigated by ^{13}C CPMAS NMR spectroscopy.
  - DSC will be used to determine glass transition, crystallization and melting temperatures as well as degree of crystallinity of the polymers.
  - DMA and tensile testing will be used to evaluate mechanical properties of polymer nanocomposites.
  - The hydrolytic degradation studies of polymer chains in nanocomposites will be carried out in 0.1 M phosphate buffer solution at pH=7.4 and 37°C. The samples will be prepared as films by melt press. Each specimen will be immersed in buffer solution and at predetermined time periods will be removed from the solution and rinsed with distilled water. The residual water will be wiped off and the samples

dried in a vacuum oven. The weight loss will be determined gravimetrically, molecular weight reduction by GPC, and reduction in mechanical strength by DMA and tensile testing

- Most importantly, for layered silicate nanocomposites the reverse ion-exchange reaction between surfactants (with and without grafted polymer) and Na^+ cations in salt water solution will be examined. The cleavage of the polymer chains from the clay platelets is expected to increase the dispersion of polymer in water and the rate of hydrolytic degradation

Highly Exfoliated Poly(ε-caprolactone)/Organo-montmorillonite Nanocomposites by in-*Situ* Polymerization

Eylem Tarkin-Tas, Shailesh K. Goswami, Bishwa R. Nayak and Lon J. Mathias*

Department of Polymer Science, University of Southern Mississippi, Hattiesburg, MS 39406-0076, USA

ABSTRACT

Poly(ε-caprolactone)/organo-modified montmorillonite nanocomposites were prepared by in-*situ* polymerization using dibutyltin dimethoxide as initiator/catalyst. The montmorillonite was first modified with 1-decyl-2-methyl-3-(11-hydroxyundecyl)imidazolium cation. The hydroxyl functionality was used for not only grafting polymer chains from the surface of the clay platelets but also grafting polymer chains to the surface by serving as a reversible chain transfer agent. The molecular weight of polymer chains was controlled by the ratio of monomer to hydroxyl content. XRD and TEM studies confirmed that highly exfoliated nanostructures were formed. The amount of inorganic component did not affect thermal behavior of the polymer matrix by DSC or TGA. The highly exfoliated clay sheets acted as nucleating agents and increased the degree of crystallinity, from 51 to 69% at 5 wt-%. DMA revealed an enhancement of storage modulus with increasing clay content. Modulus values increased by 70, 90, and 120% at clay contents of 1, 2 and 3 wt-%, respectively, at 0 °C and by 80, 120 and 150% at 30 °C.

INTRODUCTION

In the field of high performance materials, biodegradable polymer nanocomposites have been gaining interest because of their improved mechanical properties, barrier resistance, flame retardancy, solvent uptake, and rate of biodegradability as compared to pristine polymer properties. The utility of layered silicate clays such as montmorillonite to enhance polymer

properties has been correlated to high surface area-to-volume ratio and ability to interact with the polymer matrix. A variety of polymers have been used for preparation of polymer/layered silicate nanocomposites including polyamides, epoxy resins, poly(ethylene oxide), poly(vinyl alcohol), unsaturated polyesters, poly(ethylene terephthalate), poly(ethyl acrylate), silicone rubber, polypropylene, polystyrene and biodegradable polymers derived from petroleum sources as well as from natural sources such as polylactide, poly(3-hydroxy butyrate), thermoplastic starch and cellulose.[ii]

The clay sheets naturally occur in stacks. Thus, to become effective reinforcing agents they must be well dispersed in the polymer matrix. Due to hydrophilic nature of clay, their homogeneous dispersion in polymer matrices cannot be easily established. However, clays modified with organic compounds are more organophilic and hence more compatible with polymer matrices. This is generally achieved by ion-exchange reaction of the surface-bound inorganic cation with an organic onium ion, such as phosphonium[iii] or ammonium cations.[iv] These oniums generally possess either long alkyl chains or chains bearing functional groups able to either interact with the polymer or to initiate in-situ polymerization.

The preparation of polymer nanocomposites is accomplished mainly by three processes. The most economical and straightforward method is dry blending of components at pre-determined compositions and subsequent melt mixing or extrusion.[v,vi,vii,viii,ix,x,xi] Alternatively, intercalation of polymer chains into the silicate layers can be accomplished from solution.[xii,xiii] The most efficient method, however, involves intercalation of monomer into the platelets followed by polymerization; this is also called "in-*situ* polymerization".[xiv] These methods can lead to either intercalated or exfoliated morphologies or to a mixture of two or more nanostructures depending on the preparation conditions and the level of interaction of polymer matrix and clay. In intercalated structures, a few polymer chains are inserted between the clay layers without destroying their regularly alternating structure, whereas in exfoliated structures, the stacks are delaminated and individual clay sheets are dispersed randomly throughout the polymer matrix. In general, exfoliation of the layers provides nanocomposites with better properties compared to intercalated structures and such exfoliated morphologies are generally targeted.[1]

Poly(ε-caprolactone) (PCL) is a biodegradable aliphatic polyester which is synthesized by ring-opening polymerization of ε-caprolactone. It can be degraded by microorganisms and

undergoes facile hydrolysis. Its physical properties (a linear, flexible and partially crystalline polyester) and commercial availability make it very attractive not only as a substitute for non-degradable polymers but also for application in medical devices, drug delivery systems and food packaging. Property limitations of PCL arise from its low melting temperature and weak mechanical properties. The former can be overcome by blending with other polymers or by crosslinking. In order to improve thermal stability, mechanical properties, barrier properties and solvent resistance, PCL-based nanocomposites offer potential. Most attempts use montmorillonite owing to its easy availability, low cost and environmentally friendliness.[xv]

The first study on PCL based layered nanocomposites made by in-*situ* polymerization was reported by Messersmith and Giannelis. In this work the nanocomposite was synthesized by stirring Cr^{+3} exchanged fluorohectorite, a mica-type layered silicate, with caprolactone at 25 °C for 12 h fallowed by heating at 100 °C for an additional 48 h. However, x-ray powder diffraction (XRD) patterns showed intercalated nanostructures.[xvi] The same research group reported the synthesis of PCL based nanocomposites by in-situ polymerization with montmorillonite modified with protonated 12-aminolauric acid. XRD patterns of composite powders showed no sharp reflections below $2\theta = 10^{o}$ which indicates that the layers were delaminated. 12-Aminolauric acid was chosen due to the potential of carboxylic acid end groups to initiate polymerization of ε-caprolactone. However, no linear dependence of molecular weight on organically modified clay content was observed by GPC analysis of recovered polymer chains, as would be expected for such a surface-initiated system.[xvii]

More recently, the synthesis of PCL/montmorillonite nanocomposites by both melt intercalation and in-*situ* polymerization methods was reported by Dubois and coworkers. PCL based nanocomposites with different relative compositions of montmorillonite, either natural or organo-modified by various alkyl ammonium cations, were prepared. The results showed that intercalated nanostructures were obtained by melt intercalation only when organically modified montmorillonite was used, while the in-*situ* polymerization method gave more dispersion even with the unmodified natural clay.[xviii] Other studies done by the same group have shown that the type of preparation method, the nature of the surfactant or organic modifier, and the content of organo-clay affect the morphological, mechanical and thermal properties of the nanocomposites. The in-situ intercalative polymerization was found to be the most efficient method to obtain nanostructures near-to-exfoliated, and hence gave nanocomposites with much improved

properties such as gas barrier,[xix,xx] mechanical properties[xxi] and thermal properties.[xxii] In general, such near-to-exfoliated morphology is achieved when the natural clay is modified with hydroxyl group containing alkyl ammonium cations which can initiate the ring-opening polymerization of ε-caprolactone.[xxiii,xxiv] The hydroxyl groups can also be converted into metal alkoxides which can be coactivators for polymerization and lead to grafted polyester chains.[xxv]

The alkyl ammonium cations used for the preparation of polymer/organoclay nanocomposites generally exhibit poor thermal stability, especially with preparation of nanocomposites by the melt intercalation method. Thermal degradation studies of alkyl-imidazolium salts and alkyl-imidazolium modified montmorillonite showed greater thermal stability compared to all alkyl-quaternary ammonium montmorillonite.[xxvi] Polystyrene,[xxvii,xxviii,xxix] polyamide 6[xxix], poly(ethylene terephthalate),[xxx] polypropylene[xxxi] and poly(ethylene naphthalate)[xxxii] have been used to prepare nanocomposites with alkyl-imidazolium modified montmorillonite by in-*situ* polymerization, melt intercalation and solvent blending methods. However, there has been no effort to use alkyl-imidazolium modified montmorillonite with the surfactant bearing reactive functional groups for synthesis of polyester-based nanocomposites. In addition, among the functionalized quaternary alkyl-ammonium surfactants used to date, there have been no reports on terminal functional groups on the long-alkyl chains attached to the surfactant.

In this study, montmorillonite was treated with a novel alkyl-imidazolium surfactant bearing a terminal hydroxyl group on a long alkyl chain. The effect of surfactant on polymer conversion and molecular weight, polymer grafting efficiency and final nanocomposite properties such as morphological, thermal and mechanical properties was then evaluated.

EXPERIMENTAL

Materials. ε-Caprolactone was purchased from Acros (99%). Dibutyltin dimethoxide (Aldrich) was diluted with anhydrous toluene (Sigma-Aldrich). Sodium montmorillonite (MMT) with a cation exchange capacity of 93 meq/100 g was purchased from Southern Clay Products, Inc. 1-Decyl-2-methyl-imidazole and 11-bromo-1-undecanol were supplied by Aldrich and used as received. Poly(ε-caprolactone) with a melting point of 60 °C and M_n of 42500 g/mol was supplied by Aldrich. LiCl was dried in a vacuum oven prior to being used (J.T. Baker Chemical Co.). THF, ethyl ether and $CHCl_3$ were purchased from Fischer Scientific and used without

further purification.

Synthesis of 1-Decyl-2-methyl-3-(11-hydroxyundecyl)imidazolium Bromide (Surfactant). 1-Decyl-2-methylimidazole (0.95 mol) was added to an excess of 11-bromo-1-undecanol (1 mol) in a thick-walled, single neck round-bottom flask equipped with a reflux condenser. The reaction mixture was heated to 100 °C, and allowed to react for 6 h under nitrogen atmosphere. The white solid product was filtered and washed with ethyl acetate, and the solvent was removed under vacuum at 80 °C. The yield was 90%. The product was characterized by ^{1}H and ^{13}C NMR spectroscopy. ^{1}H NMR ($CDCl_3$) δ (ppm): 0.60 (t, CH_2-C$\underline{H}_3$), 1.07 (m, 15x$C\underline{H}_2$), 1.35 (m, N-CH_2-$C\underline{H}_2$), 1.64 (m, $C\underline{H}_2$-CH_2-OH), 2.63 (s, Ar-C-$C\underline{H}_3$), 3.40 (t, $C\underline{H}_2$-OH), 4.09 (t, N-CH_2), 7.46 (d, Ar-C$\underline{H}$). ^{13}C NMR ($CDCl_3$) δ (ppm): 10.8 (CH_2-$\underline{C}H_3$), 13.9 (Ar-C-$\underline{C}H_3$), 22.4, 25.5, 26.2, 29.3, 32.4 (15xCH_2), 49.1 (2xN-$\underline{C}H_2$), 62.3 ($\underline{C}H_2$-OH), 121.9 (Ar-$\underline{C}$), 142.9 (Ar-$\underline{C}$-CH_3)

Preparation of Organo-modified Montmorillonite (OMMT). The imidazolium salt (1.5 equivalent of the CEC of sodium montmorillonite, MMT) was dissolved in ethanol at 50 °C and added to a 10 wt-% aqueous, pre-dispersed suspension of sodium montmorillonite under vigorous stirring at 60 °C. The mixture was stirred for 10 h at 60 °C. The imidazolium-modified montmorillonite (OMMT) was then collected by filtration, washed several times with hot deionized water and then with hot ethanol and paper filtered. The hydroxyl alkyl-imidazolium modified montmorillonite was dried at 80 °C under vacuum for 24 h prior to use and the organic content was determined by TGA.

Preparation of PCL/OMMT Nanocomposites by in-*Situ* Intercalative Polymerization of ε-Caprolactone. The typical polymerization procedure was as follows: The desired amounts of OMMT and ε-caprolactone were added to a polymerization tube with the amount of monomer and dibutyltin dimethoxide kept constant for each polymerization vessel. The reaction mixture was stirred at room temperature for 4 h under nitrogen atmosphere. A solution of dimethyltin dimethoxide in anhydrous toluene was added (with molar ratio of monomer to catalyst adjusted to 300). The temperature was increased to 100 °C and polymerization was allowed to proceed for 24 h. The crude product was dissolved in $CHCl_3$ and centrifuged for 15 min at 3300 rpm. The

supernatant was removed and precipitated into ethyl ether. The white precipitate was filtered and dried in a vacuum oven at 40 °C.

Nanocomposites containing 1, 2, 3, 4 and 5 wt-% OMMT were prepared. The numbers in the abbreviations indicate the wt-% of OMMT (i.e. PCL1 is poly (ε-caprolactone)/clay nanocomposites with 1 wt-% of hydroxyl alkyl-imidazolium modified montmorillonite). The formation of PCL was determined by ^{1}H and ^{13} NMR in $CDCl_3$, ^{13}C solid-state NMR as well as FTIR analysis of nanocomposites. ^{1}H NMR ($CDCl_3$) δ (ppm): 1.38 (m, γ-CH_2), 1.65 (m, β-CH_2 + δ-CH_2), 2.31 (t, α-CH_2), 3.65 (ε-CH_2-OH end group), 4.02 (t, ε-CH_2). ^{13}C NMR ($CDCl_3$) δ (ppm): 24.6 (γ-CH_2), 25.6 (β-CH_2), 28.4 (δ-CH_2), 34.1 (α-CH_2), 64.2 (ε-CH_2), 173.4 (C=O). ^{13}C Solid State NMR δ (ppm): 26.3 (γ-CH_2 + β-CH_2), 29.2 (δ-CH_2), 34.2 (α-CH_2), 64.5 (ε-CH_2), 174.3 (C=O). FTIR λ^{-1} (cm^{-1}): 1727 (C=O)

Polymer Recovery from Nanocomposites. The poly(ε-caprolactone) chains were extracted from the clay by ion-exchange reaction. Thus, 1 g of the nanocomposite was suspended in 15 mL of THF and stirred for 2 h at room temperature. This solution was then poured into 1 wt-% LiCl solution in THF and stirred at room temperature for 48 h. The solution was centrifuged for 30 min and the polymer-containing supernatant was collected. The solid fraction was washed with 15 mL of THF twice and the supernatants were combined. The solvent was partially evaporated and the polymer was precipitated into ethyl ether. The white powder was dried in a vacuum oven at 40 °C.

Characterization of PCL/OMMT Nanocomposites. ^{1}H and ^{13}C NMR spectra were obtained in $CDCl_3$ using a Varian Mercury 300 spectrometer operating at 300 MHz for proton and 75 MHz for carbon. Solid-state NMR spectroscopy was performed on a Varian UNITY INOVA 400 spectrometer using a standard Chemagnetics 7.5 mm PENCIL-style probe. Samples were loaded into zirconia rotor sleeves, sealed with Teflon (TM) caps, and spun at the rate of 4.0 kHz. The acquisition parameters were as follows: The ^{1}H 90° pulse width was 4.0 μs, the cross-polarization contact time was 1 ms, the dead time delay was 6.4 μs, and the acquisition time was 45 ms. A recycle delay of 3 seconds between scans was utilized. FTIR spectra were recorded on an ATI-Mattson Galaxy 5000 FTIR spectrometer.

SEC was carried out in THF (5 mg/ mL) at 30 °C with Waters M-150-C ALC/GPC

chromatograph equipped with the Viscotek Differential Viscometer, Model 100 and Styrene-DVB GPC columns: 2xLinear+500 (flow rate: 1 ml/ min) and Hewlett-Packard 1037A refractive index detector. Molecular weight and molecular weight distributions were measured with respect to polystyrene standards.

Thermal analyses were performed on a TA instruments SDT 2960 TGA-DTA at 10 °C/min under nitrogen from ambient temperature to 700 °C and DSC 2920 at 10 °C/min under nitrogen from –90 °C to 80 °C. For DSC measurements the samples were prepared by using a melt press. They were melted at 85°C, held for 3 min at this temperature under ~3 MPa pressure, and then quickly quenched between steel plates. All samples weighed in the range of 6.0 ± 0.5 mg. The crystallization temperature (T_c), heat of crystallization (ΔH_c), crystalline melting temperature (T_m) and heat of fusion (ΔH_f) were obtained by the following procedure: the samples were cooled to -90 °C at a cooling rate of 10 °C/ min, held at this temperature for 2 min, then temperature increased to 80 °C at a rate of 10 °C/ min and equilibrated at this temperature for 5 min to erase the thermal history. The temperature was then decreased to -90 °C and again increased to 80 °C following the same procedure above.

X-ray powder diffraction (XRD) patterns were obtained using a Rigaku Ultima III X-ray diffractometer equipped with Ni-filtered CuKα radiation (wavelength λ= 1.54 Å) and operated at 40 kV and 44 mA. XRD data were recorded between 2 and 45° at steps of 2°/min. TEM images of the samples were obtained using a Zeiss EM 10-C Transmission Electron Microscope operating at an accelerating voltage of 50 kV. The ultrathin sections of the samples were taken with a microtome using a diamond knife and collected on copper grids.

Thin films of samples were prepared following the same procedure for DSC analysis. DMA measurements of the samples were carried out under tension using a TA instruments DMAQ800 at a heating rate of 2 °C/ min under nitrogen with a frequency of 1 Hz and a force of 0.1 N.

RESULTS AND DISCUSSION

Preparation of PCL/OMMT Nanocomposites. The synthesis of surfactant is schematically illustrated in Figure 1. The product was isolated by filtration with excellent yield. The chemical structure of the surfactant was determined by its ^{1}H and ^{13}C NMR spectra in $CDCl_3$.

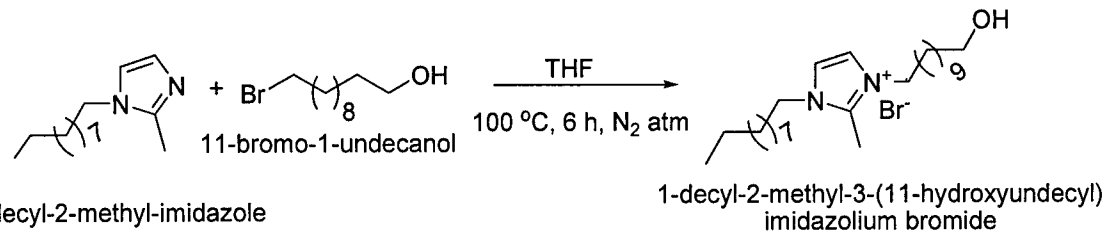

Figure 1. Synthesis of 1-decyl-2-methyl-3-(11-hydroxyundecyl)imidazolium bromide

The montmorillonite was organically modified via ion-exchange reaction between imidazolium and sodium cations with ~90% cation exchange efficiency. The organic content of the organomodified montmorillonite (OMMT) was determined as 22 wt-% by TGA. The onset decomposition temperature of bulk surfactant, 218 °C, was increased to 285 °C after incorporation onto montmorillonite. The PCL nanocomposites with 1, 2, 3, 4 and 5 wt-% OMMT content were prepared by in-situ polymerization in bulk. Dibutyltin dimethoxide was used as an initiator/catalyst for coordination insertion polymerization in which ring opening of ε-caprolactone (ε-CL) involves cleavage of the acyl-oxygen bond and the alkoxide groups form alkyl ester end groups. The hydroxyl functionality of the surfactant served as co-initiator/chain transfer agent[21] which utilizes both "grafting from" and "grafting to" techniques. The amount of monomer and dibutyltin dimethoxide was kept constant for each polymerization vessel while the hydroxyl content was increased by increasing the OMMT content. The polymerization medium became highly viscous with increasing OMMT content. The crude products were dispersed in $CHCl_3$ and centrifuged to remove the non-dispersed clay (not tethered to polymer chains). Precipitate was observed but could not be measured which indicates that almost all polymer chains are grafted onto clay surfaces and almost all clay surfaces have significant amount of bound polymer.

The formation of polymer was determined by ^{1}H, ^{13}C NMR in $CDCl_3$, ^{13}C solid state NMR as well as FTIR spectroscopy. The polymer chains were recovered via reverse ion-exchange reaction and molecular weight was determined by SEC. The theoretical molecular weights of PCL in nanocomposites were calculated by assuming that all hydroxyl groups of surfactant on the clay and the alkoxide groups of dibutyltin dimethoxide were active. Table 1 shows that the number average molecular weight M_n decreases with increasing amount of OMMT which indicates that PCL molecular weight was, in fact, controlled by the hydroxyl

content.

Table 1. Molecular Weight Determination

Sample	Conversion (%)	M_n[a] (g/mol)	M_n[b] (g/mol)	PDI
PCL1	95	27500	25400	1.66
PCL2	93	23300	26700	1.60
PCL3	94	20800	23400	1.58
PCL4	87	17200	19800	1.60
PCL5	83	14800	16700	1.28

[a] $M_n = ([\varepsilon\text{-CL}]_0/2[Sn]+[OH]) \times M_{\varepsilon\text{-CL}} \times$ %conversion

[b] M_n determined by SEC

In order to confirm that the hydroxyl functionality of the surfactant participates in ROP of ε-CL, PCL with a low degree of polymerization was synthesized by using the same surfactant under exactly the same conditions used for preparation of PCL/OMMT nanocomposites. Figure 2 represents the ^{1}H NMR spectra of ε-CL, neat surfactant and PCL plus surfactant with a target degree of polymerization of 15. The disappearance of the peak at 3.40 ppm in spectrum B and appearance of the peak at 4.22 ppm in spectrum C confirms conversion of hydroxyl group of surfactant molecules to ester linkages upon reaction with ε-CL or PCL. In addition, the integrated area under the peak 'e' was equal to the area under peak 'j' which is the end group of this low DP PCL. The degree of polymerization was determined from end-group analysis and found to be 12.

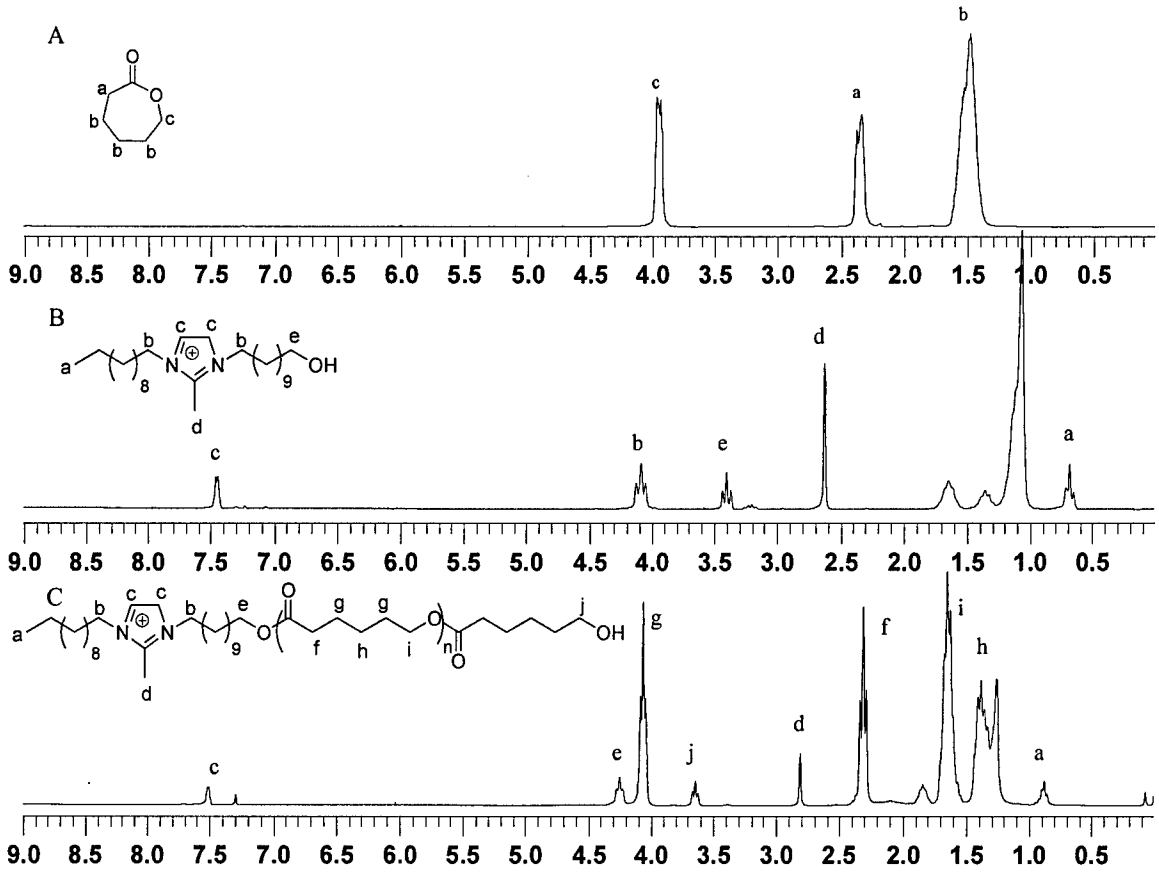

Figure 2. ^{1}H NMR spectra of A) ε-CL B) surfactant and C) PCL (DP=12)

However, the characteristic ester peak could not be seen clearly in ^{1}H NMR spectra of nanocomposites taken in $CDCl_3$. The reason might be the presence of paramagnetic species in montmorillonite (such as Fe^{3+}) which can broaden NMR peaks or the restricted mobility of surfactant bonded to montmorillonite which can make it difficult to observe peaks as well. Fortunately, after the recovery of the polymer chain by ion exchange, the corresponding peak was observed in the ^{1}H NMR spectrum at exactly the same ppm value of 4.22 (Figure 3). However, due to the high molecular weight of the PCL, the peak intensity was very low.

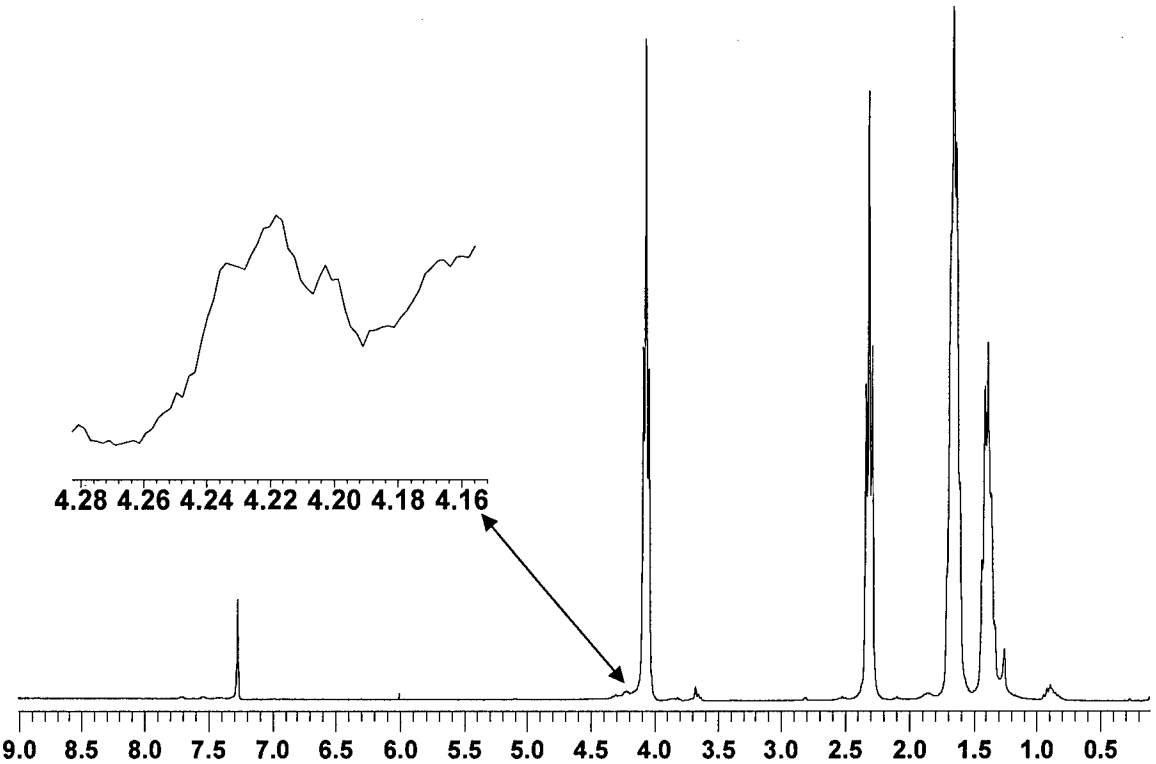

Figure 3. ^{1}H NMR spectrum of recovered PCL from PCL5

Morphological Properties. X-ray diffraction is the most commonly used technique for initial characterization of nanocomposites. XRD patterns of montmorillonite (MMT), organomodified montmorillonite (OMMT), PCL nanocomposites, and neat PCL are shown in Figure 4. The reflection at $2\theta = 7.5^{o}$, with a corresponding *d* spacing of 11.8 Å, is due to the stacked clay layers of montmorillonite. When an intercalated nanostructure is obtained, the characteristic peak of stacked layers tends to shift to the lower angle region due to expansion of *d* spacing i.e. the *d* spacing value was increased to 18.0 Å upon modification of clay with surfactant, which indicates that the intercalation of surfactant into the clay platelets took place without destroying the regular alternating structure of clay layers. In contrast, the complete disappearance of the peak was observed in the XRD patterns of the PCL nanocomposites due to loss of structural regularity of the silicate layers. The two sharp reflection peaks at $2\theta = 21.3^{o}$ and 23.7^{o} (corresponding to the crystalline structure of PCL) also appeared in the diffraction patterns of PCL nanocomposites at around the same 2θ values. Although the disappearance of the reflection peak corresponding to stacked platelets indicates a disordered structure, this does not provide the information about whether the clay platelets are fully exfoliated throughout the

polymer matrix. On the other hand, TEM analysis allows direct visualization of the morphology, spatial distribution and dispersion of nanoparticles and platelets within the polymer matrix.

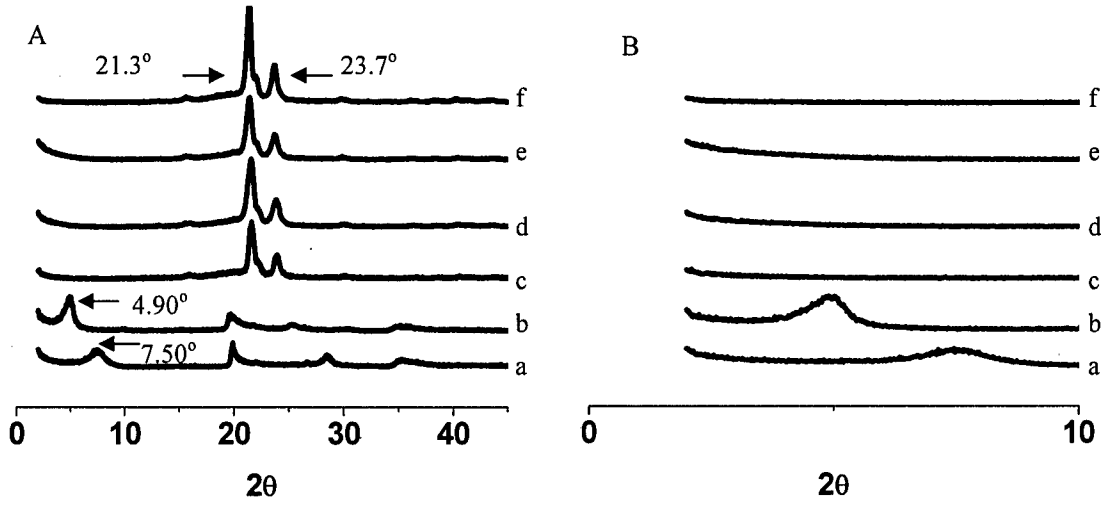

Figure 4. A) XRD patterns of a) MMT; b) OMMT; c) PCL1; d) PCL3; e) PCL5 and f) neat PCL B) expanded XRD patterns between 0 to 10°

TEM images from two different sections of PCL nanocomposite with 5 wt-% OMMT content are shown in Figure 5. It is well known that the morphology of the nanostructures is highly dependent on the interaction of the surfactant with the polymer matrix and the method for preparation of nanocomposites. Previous studies showed that near-to-exfoliated nanostructures could be achieved by using alkyl-quaternary ammonium surfactants bearing hydroxyl groups for in-situ intercalative polymerization of ε-CL.[21,22,23] However, the hydroxyl functionality of these quaternary alkyl ammonium surfactants are on short alkyl chains close to the clay surface, such as hydroxyethyl, hydroxypropyl groups. In this study the surfactant contains the hydroxyl functionality at the end of a long alkyl chain which may provide better availability of functional group for ROP of ε-CL. In other words, the mobility of the terminal hydroxyl group on the long alkyl chain is not restricted by the surface of clay which in turn may allow the monomer or PCL to easily react with it. This can increase the grafting efficiency of polymer from the surface and lead to more incorporation of polymer chains onto the clay platelets, which in turn can lead to better exfoliation. The highly exfoliated morphology of the nanocomposites can be readily seen in Figure 5, where the individual clay platelets are exfoliated and distributed throughout the polymer matrix.

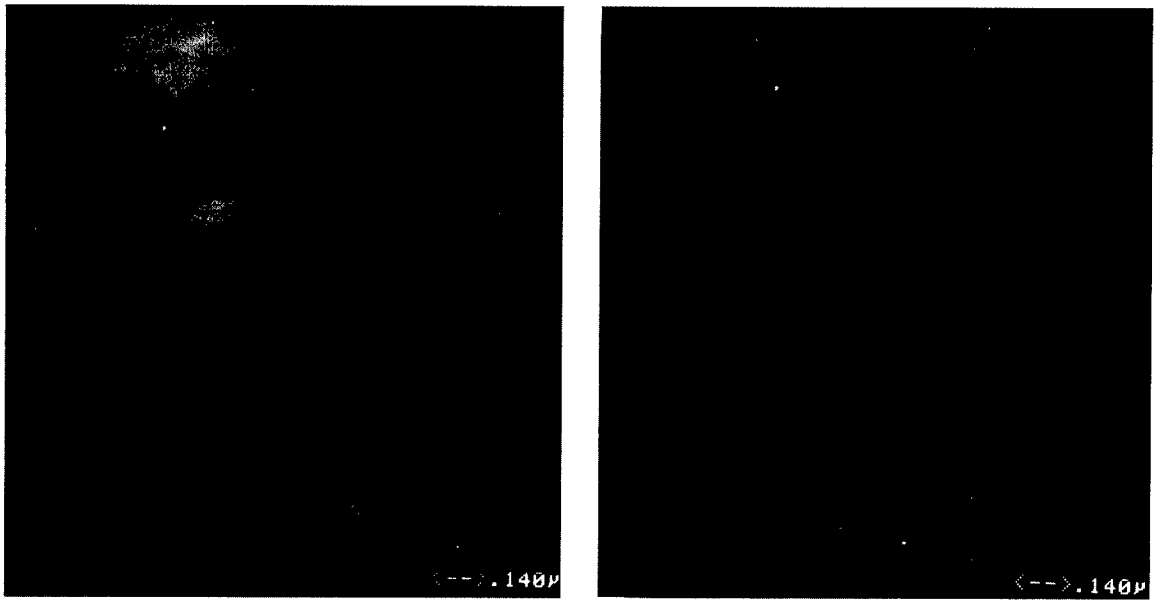

Figure 5. TEM images of PCL5 from two different sections.

Thermal Properties. The onset of thermal degradation temperatures (T_d at 2 wt-% loss) of these PCL/OMMT nanocomposites and commercial PCL were determined by TGA. The residual weights above 400 °C were in accordance with the clay content. The T_d of commercial PCL is much higher than those of nanocomposites. The reason may be due to higher molecular weight (M_n=42500) compared to the PCL chains in nanocomposites. The T_d values of nanocomposites were very close to each other and no trend with increasing clay content was observed. The increase in thermal degradation temperature with increasing clay content has been generally observed for intercalated nanocomposites.[12,xxxiii,xxxiv] The reason may be related to loss of thermal mobility and heat transfer ability of chains confined between the platelets. In this case, the clay did not show any effect on degradation temperature due to its highly exfoliated nanostructure which does not restrict thermal behavior.

The thermal properties of PCL/nanocomposites as well as commercial PCL were further investigated by DSC. Both melting and crystallization processes of PCL were detected in heating and cooling thermograms (Figure 6) of nanocomposites which indicates that the crystallization of the polymer chains was not inhibited by the inorganic component. In fact, incorporation of even 1 wt-% clay results in an obvious increase in crystallization temperature of PCL indicating that the nanolayers were able to nucleate PCL crystallization.

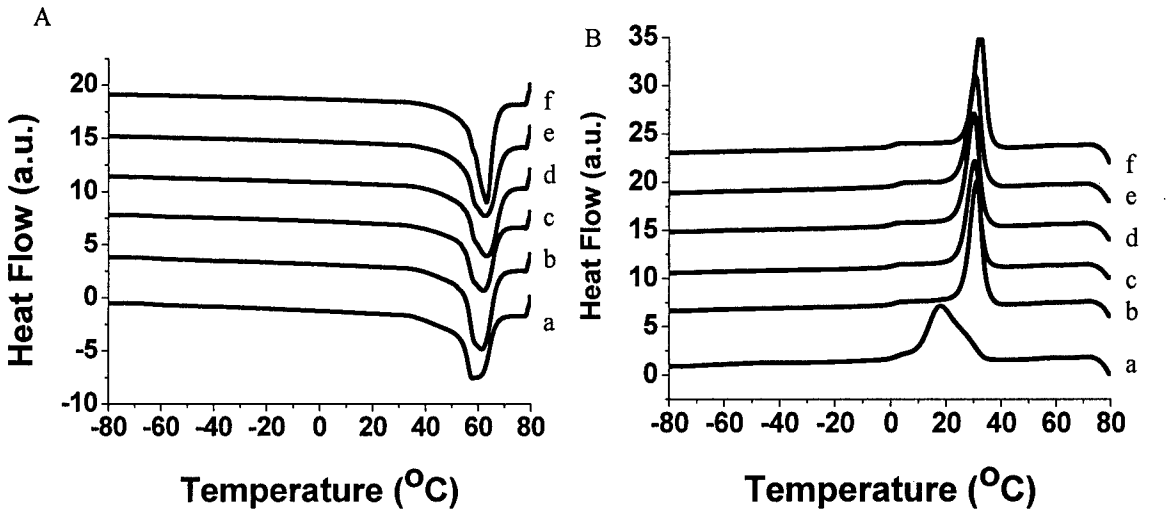

Figure 6. A) Heating Thermograms (Exo Up) of a) PCL, b) PCL1, c) PCL2, d) PCL3, e) PCL4, f) PCL5 B) Cooling Thermograms (Exo Up) of a) PCL, b) PCL1, c) PCL2, d) PCL3, e) PCL4, f) PCL5 B)

The TGA and DSC results are summarized in Table 2. The degree of crystallinity was calculated by using enthalpy of fusion (ΔH_f) for 100% crystalline PCL equal to 136 J/g[xxxv] and normalized by W_{PCL} which is the wt-% of PCL in nanocomposites (i.e. for PCL1 degree of crystallinity = $(\Delta H_{f,exp}/(W_{PCL1} x \Delta H_{f,th})) \times 100$ where W_{PCL1}=0.99). The results showed that melting and crystallization temperatures were not affected by clay content. However, an increase in degree of crystallinity was observed with increasing clay content. Previous studies showed that the degree of crystallinity is highly dependent on the morphology of nanocomposites. The absence of melting and crystallization transitions was observed by DSC measurements for PEO/montmorillonite nanocomposites in which all polymer chains were intercalated. The bulk crystallization was effectively prohibited due to confinement of the polymer chains between the layers.[xxxvi] In other studies, even though the conventional melting and crystallization curves of nanocomposites were obtained for intercalated nanocomposites by DSC, the degree of crystallinity was either not affected by clay content or decreased with increasing clay content.[9,19,xxxvii,xxxviii] The thermal properties of PCL/organically modified montmorillonite nanocomposites were investigated by Pucciarieollo et al.[xxxix] Their results showed that the presence of the organophilic clay increased the degree of crystallinity of PCL when the nanocomposites were exfoliated but reduced the degree of crystallinity when the nanocomposites

were intercalated. In this study, highly exfoliated silicate layers throughout the PCL matrix increased the surface area that can enhance nucleation and hence increased the degree of crystallinity with increasing clay content.

Table 2. Thermal Properties of PCL/OMMT Nanocomposites

Sample	T_m (°C)	ΔH_f (J/g)	T_c (°C)	ΔH_f (J/g)	Crystallinity[a] (%)	T_d (°C)
PCL[b]	58	69.9	18	65.1	51.3	342
PCL1	61	82.9	31	77.6	61.6	227
PCL2	62	75.6	30	79.3	56.7	210
PCL3	63	79.2	30	72.8	60.0	227
PCL4	62	82.4	30	75.5	63.1	219
PCL5	63	89.5	32	82.7	69.3	227

Mechanical Properties. The morphology of polymer nanocomposites has a great influence on mechanical properties. In general, the exfoliated nanostructure leads to improved mechanical properties. In addition, due to reinforcing ability of crystalline domains, the mechanical properties also tend to increase with degree of crystallinity. Figure 7 shows the storage modulus and tan δ curves as a function of temperature in the temperature range of –100°C to +50°C. The DMA of PCL4 and PCL5 was not performed because their films were brittle due to lower molecular weight of the PCL formed.

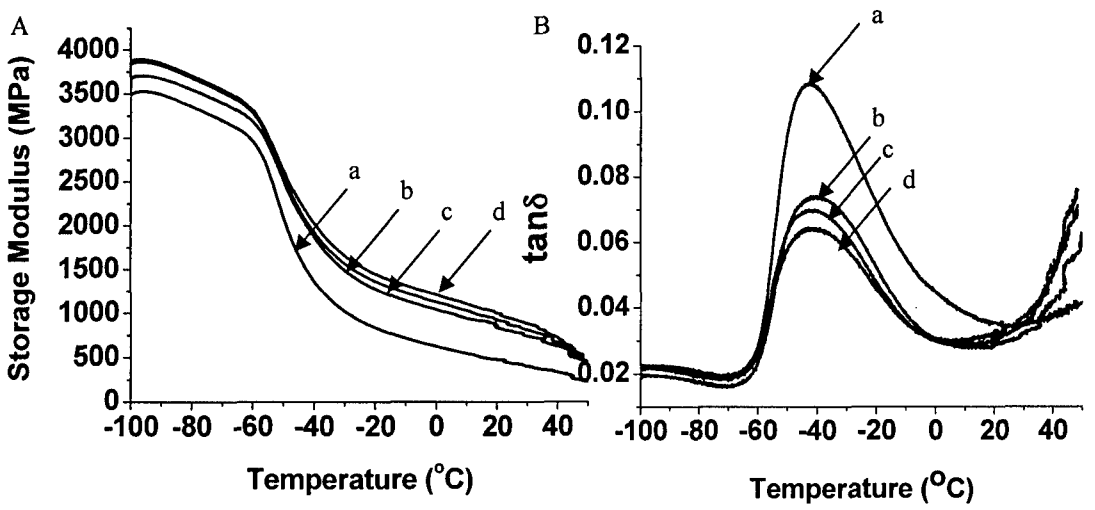

Figure 7. A) Storage Modulus vs Temperature a) PCL, b) PCL1, c) PCL2 and d) PCL3, B) tanδ vs Temperature a) PCL, b) PCL1, c) PCL2 and d) PCL3

The average values of three measurements of storage modulus at –80, 0 and 30 °C are listed in Table 3. For all nanocomposites below the glass transition temperature, the increase in storage modulus compared to neat commercial PCL is not very high. Above the glass transition temperature, however, the storage moduli of nanocomposites are obviously higher than that of PCL. Particularly, it is higher by 70%, 90% and 120% for PCL1, PCL2 and PCL3 at 0 °C. At 30 °C the increase is much higher at 80%, 120% and 150% for PCL1, PCL2 and PCL3. This indicates that the reinforcing ability of the silicate layers is significant in rubbery state. Furthermore, even though the molecular weight of PCL in nanocomposites decreases, the storage moduli increase with clay content.

Table 3. DMA Results

Sample	Storage Moduli (MPa)			T_g (°C)
	-80 °C	0 °C	30 °C	
PCL	3361	624	405	-42.4
PCL1	3551	1039	739	-42.3
PCL2	3710	1211	882	-42.7
PCL3	3842	1369	1001	-41.9

The glass transition temperature (T_g) of nanocomposites was not affected by the clay content and it is the same as that of commercial PCL. When the wt-% clay content in the nanocomposites is converted to vol-% (i.e. 1 wt-% ≅ 0.5 vol-%[10]), an effect of clay content on T_g would not be expected. However, this also indicates that no confinement of polymer chains occurred which can restrict the segmental mobility of polymer chains.

CONCLUSIONS

The molecular weight of PCL chains made by in-*situ* polymerization was controlled by the terminal hydroxyl content; i.e., by the OMMT content. The hydroxyl functionality on long alkyl chains had improved ability for grafting of polymer chains from the surface of the clay verified by the highly exfoliated morphology obtained. While this nanostructure does not affect thermal events such as T_m, T_c, T_g, and T_d, the platelets clearly act as nucleating agents for crystallization of PCL matrix and degree of crystallinity increases with clay content. Dynamic mechanical analysis revealed the enhancement of storage moduli, particularly above T_g, upon increasing the clay content.

Acknowledgment. The Office of Naval Research is gratefully acknowledged for financial support.

REFERENCES

[i] Yukie Akutsu, Toshiaki Nakajima-Kambe. *Appl Environ Microbiol,* **1998,** 64, 62.
[ii] Mai, Y. W.; Yu, Z. Z. "Polymer Nanocomposites" Woodhead Publishing Limited and CRC Press LLC, **2006.**
[iii] Imal, Y.; Inukai, Y; Tateyama, H. "Properties of Poly(ethylene terephthalate)/Layered Silicate Nanocomposites Prepared by Two-Step Polymerization Procedure" *Polymer J.* **2003**, 35, 230-235.
[iv] Usiki, A.; Kawasumi, M.; Kojima, Y.; Okada, A.; Karauchi, T; Kamigaito, O. "Swelling Behavior of Montmorillonite Cation Exchanged for ω-Amino Acids by ε-Caprolactam" *J. Mat. Res.* **1993**, 8, 1174-1178.
[v] Vaia, R. A.; Ishii, H.; Giannelis, E. P. "Synthesis and Properties of Two-Dimensional Nanostructures by Direct Intercalation of Polymer Melts in Layered Silicates" *Chem. Mater.* **1993**, 5, 1694-1696.
[vi] Ray, S. S.; Maiti, P.; Okamoto, M.; Yamada, K.; Ueda, K. "New Polylactide/Layered Silicate Nanocomposites. 1. Preparation, Characterization, and Properties" *Macromolecules* **2002**, 35, 3104-3110.
[vii] Lepoittevin, B.; Devalckenaere, M.; Pantoustier, N.; Alexandre, M.; Kubies, D.; Calberg, C.; Jerome, R.; Dubois, P. "Poly(ε-caprolactone)/Clay Nanocomposites Prepared by Melt Intercalation: Mechanical, Thermal and Rheological Properties" *Polymer* **2002**, 43, 4017-4023.
[viii] Kwap, S. Y.; Oh, K. S. "Effect of Thermal History on Structural Changes in Melt-Intercalated Poly(ε-caprolactone)/Organoclay Nanocomposites Investigated by Dynamic Viscoelastic Relaxation Measurements" *Macromol. Mater. Eng.* **2003**, 288, 503-508.

[ix] Nam, J. Y.; Ray, S. S.; Okamoto, M. "Crystallization Behavior and Morphology of Biodegradable Polylactide/Layered Silicate Nanocomposite" *Macromolecules* **2003**, 36, 7126-7131.
[x] Di, Y.; Iannace, S.; Maio, E. D.; Luigi Nicolais, L. "Nanocomposites by Melt Intercalation Based on Polycaprolactone and Organoclay" *J. Polym. Sci. Part B: Polym. Phys.* **2003**, 41, 670-678.
[xi] Chen, B.; Evans, J. R. G. "Poly(ε-caprolactone) –Clay Nanocomposites: Structure and Mechanical Properties" *Macromolecules* **2006**, 39, 747-754.
[xii] Aranda, P.; Hitzky, E. R. "Poly(ethylene oxide)-Silicate Intercalation Materials" *Chem. Mater.* **1992**, 4, 1395-1403.
[xiii] Lim, S. T.; Hyun, Y. H.; Choi, H. J.; Jhon, M. S. "Synthetic Biodegradable Aliphatic Polyester/ Montmorillonite Nanocomposites" *Chem. Mater.* **2002**, 14, 1839-1844.
[xiv] Kojima Y, Usuki, A, Kawasami M, Okada A, Fukushima Y, Kurauchi T, Kamigaito O, "Mechanical Properties of Nylon 6-Clay Hybrid" *J. Mater. Res.* **1993**, 8, 1185-1189.
[xv] Pandey, J. K.; Reddy, K. R.; Kumar, A. P.; Singh, R. P. "An Overview on the Degradability of Polymer Nanocomposites" *Polym. Degrad. Stab.* **2005**, 88, 2, 234-250.
[xvi] Messersmith, P. B.; Giannelis, E. P. "Polymer-Layered Silicate Nanocomposites: In Situ Intercalative Polymerization of ε-Caprolactone in Layered Silicates" *Chem. Mater.* **1993**, 5, 1064-1066.
[xvii] Messersmith, P. B.; Giannelis, E. P. "Synthesis and Barrier Properties of Poly(ε-caprolactone)-Layered Silicate Nanocomposites" *J. Polym. Sci. Part A: Polym. Chem.* **1995**, 33, 1047-1057.
[xviii] Viville, P.; Lazzoroni, R.; Pollet, E.; Alexandre, M.; Dubois, P.; Borcia, G.; Pireaux, J. J. "Surface Characterization of Poly(caprolactone)-Based Nanocomposites" *Langmuir* **2003**, 19, 9425-9433.
[xix] Gorrasi, G.; Tortora, M.; Vittoria, V.; Pollet, E.; Lepoittevin, B.; Alexandre, M.; Dubois, P. "Vapor Barrier Properties of Polycaprolactone Montmorillonite Nanocomposites: Effect of Clay Dispersion" *Polymer* **2003**, 44, 2271-2279.
[xx] Gain, O.; Espuche, E.; Pollet, E.; Alexandre, M.; Dubois, P. "Gas Barrier Properties of Poly(ε-caprolactone)/Clay Nanocomposites: Influence of the Morphology and Polymer/Clay Interactions" *J. Polym. Sci. Part B: Polym. Phys.* **2005**, 43, 205-214.
[xxi] Gorrasi, G.; Tortora, M.; Vittoria, V.; Pollet, E.; Lepoittevin, B.; Alexandre, M.; Dubois, P. "Physical Properties of Poly(ε-caprolactone) Layered Silicate Nanocomposites Prepared by Controlled Grafting Polymerization" *J. Polym. Sci. Part B: Polym. Phys.* **2004**, 42, 1466-1475.
[xxii] Lepoittevin, L.; Pantoustier, N.; Devalckenaere, M.; Alexandre, M.; Kubies, D.; Calberg, C.; Jerome, R.; Dubois, P. "Poly(e- caprolactone)/Clay Nanocomposites by In-Situ Intercalative Polymerization Catalyzed by Dibutyltin Dimethoxide" *Macromolecules* **2002**, 35, 8385-8390.
[xxiii] Kubies, D.; Pantoustier, N.; Dubois, P.; Rulmont A.; Jerome, R. "Controlled Ring Opening Polymerization of ε-Caprolactone in the presence of Layered Silicates and Formation of Nanocomposites" *Macromolecules* **2002**, 35, 3318-3320.
[xxiv] Lepoittevin, L.; Pantoustier, N.; Alexandre, M.; Calberg, C.; Jerome, R.; Dubois, P. "Layered Silicate/Polyester Nanohybrids by Controlled Ring-Opening Polymerization" *Macromol. Symp.* **2002**, 183, 95-102.
[xxv] Polet, E.; Delcourt, C.; Alexandre, M.; Dubois, P. "Organic Inorganic Nanohybrids Obtained by Sequential Copolymerization of ε-Caprolactone and L,L-Lactide from Activated Clay Surface" *Macromol. Chem. Phys.* **2004**, 205, 2235-2244.
[xxvi] Awad, W. H.; Gilman, J. W.; Nyden, M.; Haris, R. H.; Sutto, Jr. T. E.; Callahan, J.; Truvole, P. C.; DeLong, H. C.; Fox, D. M. "Thermal Degradation Studies of Alkyl-Imidazolium Salts and Their Application in Nanocomposites" *Thermochimica Acta* **2004**, 409, 3-11.
[xxvii] Gilman, J. W.; Awad, W. H.; Davis, R. D.; Shields, J.; Haris, R. H.; Davis, Jr. C.; Morgan, A. B.; Sutto, T. E.; Callahan, J.; Truvole, P. C.; DeLong, H. C. "Polymer/Layered Silicate Nanocomposites from Thermally Stable Trialkylimidazolium-Treated Montmorillonite" *Chem. Mater.* **2002**, 14, 3776-3785.
[xxviii] Bottino, F. A.; Fabbri, E.; Fragala, I. L.; Malandrino, M.; Orestano, A.; Pilati, F.; Pollicino, A. "Polystyrene-Clay Nanocomposites Prepared with Polymerizable Imidazolium Surfactants" *Macromol. Rapid Comm.* **2003**, 24, 1079-1084.
[xxix] Morgan, A. B.; Harris, J. D. "Exfoliated Polystyrene-Clay Nanocomposites Synthesized by Solvent Blending with Sonication" *Polymer* **2004**, 45, 8695-8703.
[xxx] Davis, C. H.; Mathias, L. J.; Gilman, J. W.; Schiraldi, D. A.; Shields, J. R.; Truvole, P.; Sutto, T. E.; Delong, H. C. "Effects of Melt Processing Conditions on Quality of Poly(ethylene terephthalate) Montmorillonite Clay Nanocomposites" *J. Polym. Sci. Part B: Polym. Phys.* **2002**, 40, 2661-2666.

[xxxi] He, A.; Hu, H.; Huang, Y.; Dong, J. Y.; Han, C. C. "Isotactic Polypropylene/Monoalkyl Imidazolium-Modified Montmorillonite Nanocomposites: Preparation by Intercalative polymerization and Thermal Stability Study" *Macromol. Rapid Comm.* **2004**, 25, 2008-2013.

[xxxii] Chua, Y. C.; Lu, X.; Wan, T. "Polymorphism Behavior of Poly(ethylene naphthalate)/Clay Nanocomposites" *J. Polym. Sci. Part B: Polym. Phys.* **2006**, 44, 1040-1049.

[xxxiii] Lepoittevin, B.; Devalckenaere, M.; Pantoustier, N.; Alexandre, M.; Kubies, D.; Calberg, C.; Jerome, R.; Dubois, P. "Poly(ε-Caprolactone)/Clay Nanocomposites Prepared by Melt Intercalation: Mechanical, Thermal and Rheological Properties" *Polymer* **2002**, 43, 4017-4023.

[xxxiv] Lepoittevin, B.; Pantoustier, N.; Devalckenaere, M.; Alexandre, M.; Calberg, C.; Jerome, R.; Henrist, C.; Rulmont, A.; Dubois, P. "Polymer/Layered silicate Nanocomposites by Combined Intercalative Polymerization and Melt Intercalation: A Masterbatch Process" *Polymer*, **2003**, 44, 2033-2040.

[xxxv] Crescenzi, V.; Manzini, G.; Calzolari, G.; Borri, C. "Thermodynamics of Fusion of Poly-β-Propiolactone and Poly-ε-Caprolactone. Comparative Analysis of the Melting of Aliphatic Polylactone and Polyester Chains" *Eur.Polym. J.* **1972**, 8, 449-463.

[xxxvi] Vaiva, R. A.; Sauer, B. B.; Tse, O. K.; Giannelis, E. P. "Relaxation of Confined Chains in Polymer Nanocomposites: Glass Transition Properties of Poly(ethylene oxide) Intercalated in Montmorillonite" *J. Polym. Sci. Part B: Polym. Phys.* **1997**, 35, 59-67.

[xxxvii] Jimenez, G.; Ogata, N.; Kawai, H.; Ogihara, T. "Structure and Thermal Mechanical Properties of Poly(ε-caprolactone) –Clay Blend" *J. Polym. Sci. Part B: Polym. Phys.* **1997**, 64, 2211-2220.

[xxxviii] Tortora, M.; Vittoria, V.; Galli, G.; Ritrovati, S.; Chiellini, E. "Transport Properties of Modified Montmorillonite-Poly(ε-caprolactone) Nanocomposites" *Macromol. Mater. Eng.* **2002**, 287, 243-249.

[xxxix] Pucciarieollo, R.; Villani, V.; Belviso, S.; Gorrasi, G.; Tortora, M.; Vittoria, V. "Phase Behavior of Modified Montmorillonite-Poly(ε-caprolactone) Nanocomposites" *J. Polym. Sci. Part B. Polym. Phys.* **2004**, 42, 1321-1332.